The role of β-cell keratins in islet histology, glucose uptake, and diabetes susceptibility

Petar Kosijer

Master's thesis

University of Turku
Faculty of Medicine

31.08.2023.

Master's degree in Biomedical Imaging
Light Microscopy Imaging

Credits: 20 ECTS

Supervisors:
Diana Toivola, PhD, associate professor
Sarah Baghestani, MSc

UNIVERSITY OF TURKU
Faculty of Medicine

Petar Kosijer: The role of β-cell keratins for glucose uptake, islet histology, and diabetes susceptibility

Master's thesis
Specialization level: Light Microscopy Imaging
August 2023, pp. 56

β-cells along with several types of other cells compose the endocrine pancreas and they produce the hormone insulin which has a role in the regulation of glucose in the bloodstream. A disruption in insulin production and its secretion in β-cells causes diabetes. Keratins (K) are members of the intermediate filament protein family and they are known for both mechanical and physiological activity in cells. Their role is emphasized by 80 human diseases caused by keratin filament mutations. The most common types of keratins in the endocrine pancreas are K8 and K18 and the global K8 knockout in mice leads to the mislocalization of glucose transporter 2 (GLUT2). Three aims were set for this thesis: evaluate the connection between keratins and proliferation in β-cells, study the role of keratins in β-cells during streptozotocin-induced diabetic stress, and understand the role of keratins in β-cells during glucose uptake. Histology analysis showed that bigger islets are present in β-cell-specific K8 knockout mice compared to the wild type. The analysis of β-cell proliferation-related parameters showed no difference in these mice compared to the control. Digital and quantitative histological analysis of the samples from short-term streptozotocin-treated mice showed the K8 conditional knockout mice have lower islet damage compared to the control and were thus, less susceptible to this diabetic model. No differences were seen in islet size, islet mass, and islet number in streptozotocin-treated mice compared to control. GLUT2 localization analysis showed that in β-cell-specific K8 knockout mice GLUT2 gets mislocalized from the membrane to the cytoplasm compared to the control mice. The assessment of the damage score and GLUT2 localization analysis showed that keratins might have a role in the targeting of β-cell GLUT2 since streptozotocin is transported into beta cells through GLUT2.

Keywords: keratins, endocrine pancreas, glucose transporter 2, streptozotocin, proliferation

Abbreviation List

AUC – area under curve

DAPI – 4’,6’-diamidino-2-phenylindole

ER – endoplasmic reticulum

GLUT – glucose transporter

GLUT2 – glucose transporter 2

GSIS – glucose-stimulated insulin secretion

IF – intermediate filaments

K – keratin

OCT – optimal cutting temperature compound

PFA – paraformaldehyde

STZ – streptozotocin

T1D – type 1 diabetes

T2D – type 2 diabetes

UPR – unfolded protein response

YAP – Yes-associated protein

Table of Contents

1. Literature review

1.1. Pancreas

Pancreas consists of the exocrine and endocrine part which have distinct, but interconnected roles. The exocrine pancreas is built up of acinar and duct cells and their main role is to secrete enzymes and assimilate nutrients into the body. Acinar cells account for the synthesis of digestive enzymes such as trypsin, lipase, and amylase, while in duct cells, sodium bicarbonate is generated (Atkinson et al., 2020). On the other hand, several types of cells build up the endocrine pancreas and their role is the secretion of hormones responsible for the maintenance of normal blood glucose levels. Comparing both the exocrine and endocrine pancreas, the exocrine pancreas accounts for almost 80% of the organ (Leung, 2010). From an anatomical perspective, the pancreas is located in the upper abdomen retroperitoneally and is connected with several organs: the spleen, stomach, duodenum, and colon (Leung, 2010). When it comes to organization, three parts of the pancreas can be distinguished: head, body, and tail. The head is juxtaposed next to the duodenum, and the tail is near the spleen and contains pancreatic polypeptide which is a precursor for peptide hormone. Compared with a human pancreas, the murine pancreas is distributed within the mesentery in the proximity of the small intestine and three lobes can be distinguished: duodenal, splenic, and gastric lobe (Figure 1) (Dolenšek et al., 2015). Lobes are separated by adipose and connective tissue between each other.

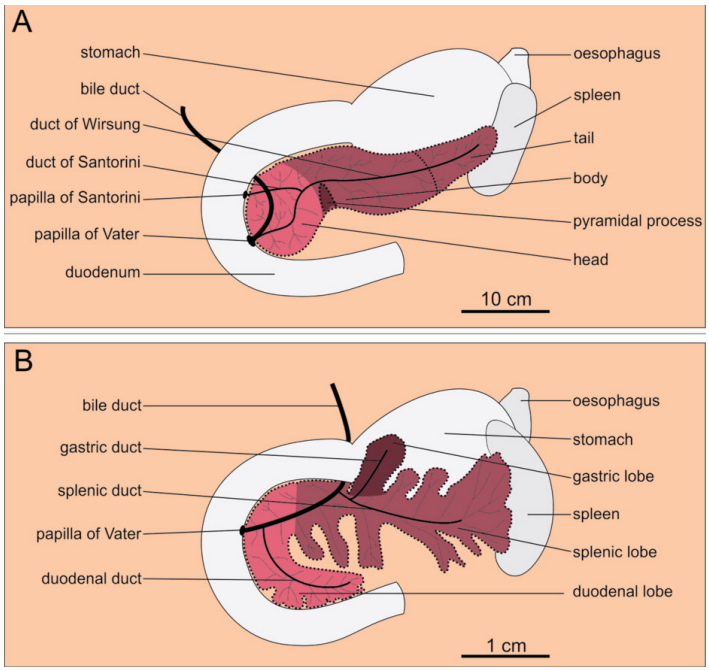

Figure 1: Anatomical comparison between human (A) and mouse (B) pancreas with specific structures (from Dolenšek et al., 2015)

From an embryological point of view, the development of the pancreas goes through processes of organ specification, expansion, differentiation, and maintenance, it is known that these processes overlap throughout the development (Murtaugh, 2008). The

differentiation into the exocrine and endocrine pancreas is a complex process that is controlled by multiple transcriptional factors. Regarding the endocrine pancreas, it is obvious during the 12th week of development and the hormone-expressing structures are seen one week later. However, the whole process of pancreas maturation occurs after birth. The pancreas is innervated by motor nerves that send impulses to both the exocrine and endocrine pancreas (Atkinson et al., 2020). Parasympathetic nerves are responsible for sending impulses for the normal functioning of both pancreatic compartments, while impulses coming from sympathetic ones inhibit these functions. In summary, the activity of both parts is regulated by the autonomic nervous system, metabolites, and hormones.

1.1.1. Endocrine pancreas and β-cells

The endocrine pancreas consists of cells that are organized into clusters known as islets of Langerhans (Figure 2). Islets are scattered all over the pancreas due to the lack of compartmentalizing structures and represent up to 2% of the total mass of the pancreas. The human pancreas has approximately 1 million islets and their role, as previously mentioned, is to contribute to glucose homeostasis. It is important to emphasize that the endocrine pancreas is more vascularized than the exocrine pancreas, which also facilitates the role of maintaining optimal glucose levels and the endocrine pancreas receives 10% of the blood supply required for the whole pancreas (Rorsman and Braun, 2013). The blood supply is achieved by multiple arterioles and further branched capillaries which later assemble into veins outside of the islets.

Five major cell types constitute the endocrine pancreas: α-cells, β-cells, δ-cells, F-cells, and in a significantly low percentage, epsilon cells. Every type of cell is responsible for the synthesis and secretion of hormones which are essential for physiology and nutrient homeostasis: α-cells account for the production of glucagon, β-cells secrete insulin, δ-cells are known for the synthesis of somatostatin, F-cells for the production of pancreatic polypeptide, and epsilon cells, the least distributed cells in the endocrine pancreas, secrete ghrelin (Kulkarni, 2004). On a microscopic level, a structural difference between cells of human and murine endocrine pancreas exists: islets in humans are located intralobular, while in mice interlobular and there is a possible explanation for this difference: in larger animals, such as humans, lobules are formed by fusion of existing smaller lobules leading to the change from previously interlobular islets into intralobular (Dolenšek et al., 2015). Also, the distribution of cells is different in both humans and mice: α-cells are scattered within islets in humans, while in mice they are assembled into a ring-like structure

surrounding beta (β) and other cell types. β-cells are the most abundant cell type in the endocrine pancreas and they account for almost 80% of all islet cells (Leung, 2010). The development of β-cells within the endocrine pancreas takes place from a specific precursor cell: the cell is hormone-containing, meaning that other hormones than insulin can be found, and starts to migrate into surrounding tissue and assemble into clusters with other cells (Herrera et al., 2002). Endocrine progenitor cell needs several transcription factors to be further developed into β-cells: Pdx1, Ngn3, and Pax6 (Herrera et al., 2002). Mature β-cells are responsible for monosaccharide uptake and metabolism, especially for glucose, but also galactose and mannose can be processed in β-cells.

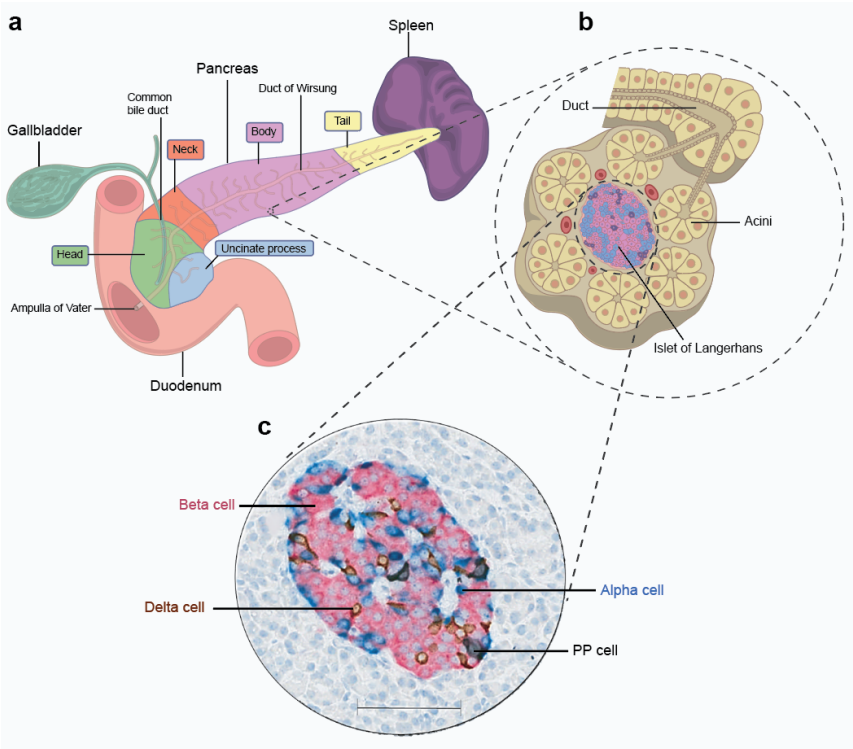

Figure 2: Organization of human pancreas (A) with the close-up of exocrine and endocrine pancreas (B) and the close-up of the islet of Langerhans with its cell types (C) (from Atkinson et al., 2020)

Insulin, the main hormone produced by β-cells, is responsible for the decrease of blood glucose levels by enhancing glucose uptake in adipose and other peripheral tissues. It is a 51 amino acid peptide made up of A and B chains linked by 2 disulfide bonds which are derived from cysteine residues (Figure 3) (Rachdaoui, 2020). The active form of insulin is achieved by successive cleavage of its precursor peptides: preproinsulin and proinsulin. Preproinsulin is cleaved just before the endoplasmic reticulum, and proinsulin is converted to insulin in the endoplasmic reticulum where prohormone convertase catalyzes this process (Leung, 2010). Autocrine interactions explain the activity of insulin and this is characterized by both benefits and limiting outcomes. The positive actions of insulin on β-cells include activation of insulin transcription and translation and rapid

insulin secretion upon these events. Along with this, insulin affects β-cell growth and survival by activation of anti-apoptotic mechanisms. On the other hand, observed negative actions of insulin include an inhibitory feedback loop on its production (Rachdaoui, 2020).

Figure 3: Structure of insulin (PDB ID: 3I40) with chain A built of 21 amino acids (light green) and chain B built of 30 amino acids (orange). In the structure, disulfide bonds derived from cysteine residues (emphasis on yellow) are seen (Timofeev et al., 2010)

1.1.2. Proliferation rate in β-cells

A main feature of β-cells is that they are long-living cells with a low replication rate (estimated 0.1-0.5%) during adulthood. Most β-cells are formed during embryogenesis and the replication rate is significantly decreased after birth and infancy (Shcheglova et al., 2022). This decrease also relates to the number of cells going from the G1 to the S phase. The replication rate in β-cells decreases with age and is reversely proportional to the maturation. Regarding cell proliferation in β-cells, research showed differences in gene expression between embryonic and post-weaning β-cells related to expansion and maintenance. For example, a transcription factor MafB was shown as relevant in the development of β-cells but postnatally was expressed in glucagon-secreting alpha cells. Along with MafB, connective tissue growth factor was expressed during the development of β-cells in infancy, but not in adulthood (Artner et al., 2007; Gunasekaran et al., 2012). The role of cyclin D2 in terminally differentiated β-cells during replication has been emphasized to contribute to an increase of β-cell mass. Cyclin D2 in β-cells serves as a

component in mitogen signaling and link in cell machinery, and the evidence showed that dependent kinases essential for proliferation of β-cells were less distributed in cyclin D2 knockout mice (Georgia and Bhushan, 2004). The capacity of β-cells to replicate is limited and usually, this is during various states of metabolic demands: such as obesity, pregnancy, and injury. A low replication rate among β-cells can be explained by their environment: β-cells are interspersed within the exocrine pancreas, which is a toxin- and mechanostress-free environment, compared to the liver and intestine, which are exposed to both toxins and shear stress (Shcheglova et al., 2022). Most of the processes within β-cells are determined by the ER-stress-induced unfolded protein response, abbreviated UPR. Under conditions of increased insulin production and ER stress, unfolded protein response initiates apoptosis in β-cells (Shcheglova et al., 2022). To boost β-cell proliferation to combat diabetes and increase the number of β-cells, mitogen-related research has been conducted in mice, but in humans, the outcome was different due to the failure of mitogens from mice to induce a proliferative effect in humans. Also, it should be emphasized that the machinery required for cell cycles differs between humans and mice. Cyclin-dependent kinase 6 is absent in rodents but is necessary for the proliferation of β-cells in humans (Fiaschi-Taesch et al., 2010).

Yes-associated protein (YAP) is known as a transcriptional coactivator and effector of the Hippo signaling pathway (Uttagomol et al., 2019). Its phosphorylation upon Hippo signaling causes exclusion from the nucleus.

1.2. Diabetes

Diabetes is infamously known as one of the most common and most concerning diseases in modern society and different factors are known for causation and further contribution to diabetes. Type 1 diabetes (T1D) is an autoimmune disease caused by the destruction of β-cells and the underlying causes are genetic and environmental factors, and type 2 diabetes (T2D) with a complex mechanism mostly related to insulin resistance (Shcheglova et al., 2022). In T1D, the first signs of autoimmunity include seroconversion of autoantibodies to insulin and glutamate decarboxylase and the development of an inflammatory environment similar to insulitis (Roep et al., 2021). Another causation for T1D is seen in β-cells as well and several factors that trigger a β-cell-induced immune response have been documented: besides metabolic stress, viral infections, and inflammatory gut agents that leak into the pancreas can create an inflammatory environment (Roep et al., 2021). Genetic studies identified the insulin gene as one of the factors that contribute to genetic susceptibility to the T1D (Bell et al., 1984). Furthermore,

15 other genes have been associated with the development of type 1 diabetes, and 2 of them are related to the activation of T-cells (Gillespie, 2006). Both types of diabetes lead to hyperglycemia. T2D is characterized by significantly reduced β-cell mass compared to the normal pancreas: loss of up to 60% was reported in autopsy studies (Westermark et al., 1987). It is still questionable if T2D has roots in genetic predisposition or contemporary lifestyle. Another finding that contributes to the research of diabetes is the fat content in patients: it has been confirmed that the increase of fat and its accumulation in organs is a sign of β-cell function disruption.

1.2.1. Glucose-stimulated insulin secretion (GSIS)

The main mechanism that connects both glucose uptake and insulin release is known as glucose-stimulated insulin secretion (GSIS) (Figure 4) (Leung, 2010). It starts with the entry of glucose molecules facilitated by glucose transporter proteins (GLUTs) and upon the entry glucose goes through glycolysis and the Krebs cycle yielding ATP and coenzyme A. As the ratio ATP/ADP is increased, the membrane gets depolarized leading to the inhibition of K^+ channels. Furthermore, voltage-dependent Ca^{2+} channels open causing an influx of Ca^{2+} ions leading to exocytosis and release of insulin into the bloodstream. An impairment of glucose homeostasis, an inability of β-cells to produce insulin and an inefficient number of β-cells lead to diabetes.

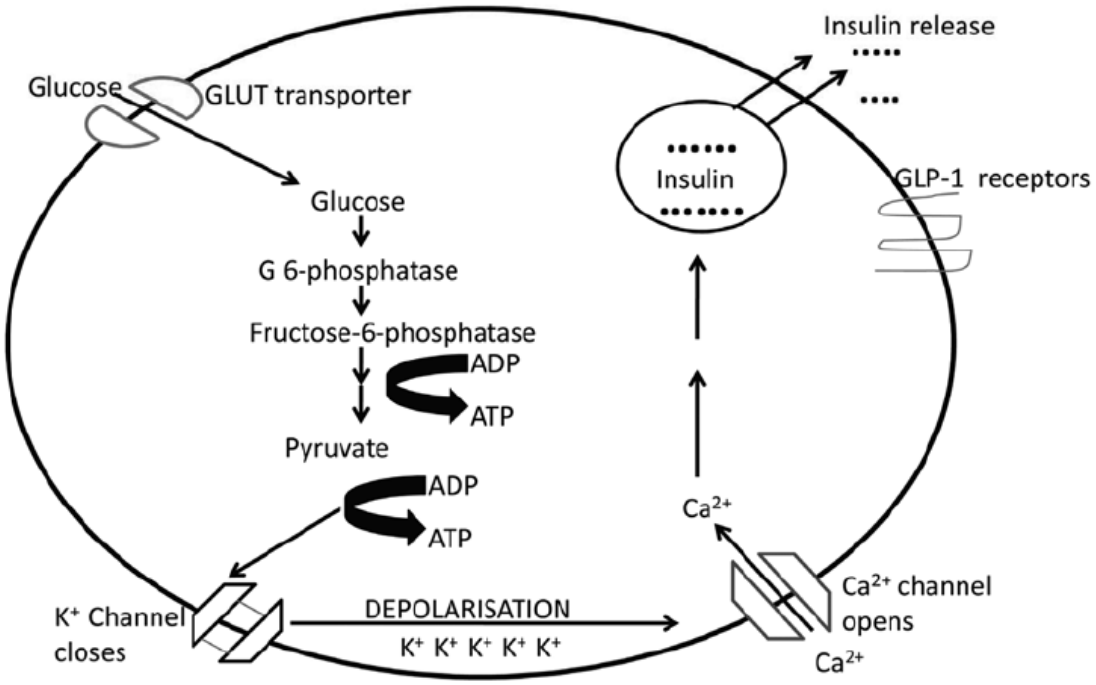

Figure 4: A simplified graph showing processes of glucose uptake and glucose-stimulated insulin secretion. The glucose enters the cell via glucose transporter (GLUT) proteins and gets processed to pyruvate in glycolysis, after which pyruvate enters mitochondria and the Krebs cycle occurs. After

generating ATP, the potassium channels close, leading to a depolarization and opening of calcium channels. The influx of Ca^{2+} ions pushes insulin vesicles to the membrane resulting in the secretion and release of insulin (Baur et al., 2012)

1.2.2. Glucose transporters

Glucose transporters (GLUTs) are integral membrane proteins that facilitate the transport of monosaccharides, especially the transport of glucose and smaller compounds into the cell. These proteins are encoded by the *SLC2* gene and belong to the major facilitator superfamily (Mueckler and Thorens, 2013). In humans, 14 GLUT proteins have been identified and they are characterized by specific affinities towards specific substrates. Approximately 500 amino acids are involved in constituting a single glucose transporter and three classes can be distinguished based on sequence similarity: Class 1 counts for GLUTs 1-4, Class 2 for GLUTs 5, 7, 9, and 11, while Class 3 includes GLUTs 6, 8, 10, 12 and HMIT transporter (Mueckler and Thorens, 2013). In regards to the structure of GLUT proteins, several regions can be found: 12 transmembrane segments, a single site for N-linked glycosylation, cytoplasmic linker domain, and cytosolically located N- and C-termini. GLUT2 is characterized by a low affinity for glucose, whose Km value stands approximately around 17 mM and this is considered a unique feature among GLUT proteins (Mueckler and Thorens, 2013). GLUT2 has a broad distribution in the human body: this protein can be found in hepatocytes, intestine, kidneys, β-cells of the pancreas, and neurons.

1.2.2.1. Glucose transporter 2 (GLUT2) in the endocrine pancreas

In human β-cells, GLUT2 along with GLUT1 and GLUT3 transports glucose, while in rodents GLUT2 is the main glucose transporter. The expression and distribution of GLUT2 in β-cells depend on the content of glucose and lipids, and in the case of glucotoxicity or lipotoxicity, the surface expression of GLUT2 is reduced. The underlying mechanism of reduced GLUT2 expression is seen in the downregulation of glycosyltransferase enzyme which assembles GLUT2 with the galectin 9 molecule located on the membrane. The presence of galectin 9 is essential for the function of GLUT2, as it is a molecule interacting with the N-glycan-specific structure of the GLUT2 (Berger and Zdzieblo, 2020). The knockout of the *Slc2a2* gene which encodes GLUT2 leads to a disorder known as Fanconi-Bickel syndrome characterized by glucose uptake impairment and impaired insulin secretion (Berger and Zdzieblo, 2020). The insulin secretion disruption is more emphasized in mice than in humans, as the absence of GLUT2 is compensated by the efficiency of GLUT1 and GLUT3 transporters. The

knockout of the *Slc2a2* gene in mice leads to a later insulin response to hyperglycemic stimuli and the absence of the primary response pathway indicates that the presence of other GLUT proteins is not sufficient to reach a required glucose uptake threshold. In humans, glucose uptake is predominately exerted by GLUT1 and GLUT3, which has been confirmed by Segerstolpe et al. after analyzing the expression of *SLC2* genes and RNA sequencing (Segerstolpe et al., 2016). They showed that both levels of mRNA and protein content for GLUT1 and GLUT3 were higher than the ones for GLUT2. The role of GLUT2 in human β-cells is also significant along with GLUT1 and GLUT3 (Ohtsubo et al., 2011). The simultaneous knockdown of *Slc2a1* and *Slc2a2* genes showed a bigger reduction of glucose uptake, as the individual knockdown showed no significant difference (Ohtsubo et al., 2011). The expression of the *Slc2a2* gene is shown to be executed in a glucose-dependent manner and a confirmation of this mechanism was also achieved by using other metabolites which mimicked glucose, where it was shown that the gene expression is regulated by glucose metabolism and not by interactions between substrates and the transporter (Ferrer et al., 1993). In regards to a nutrient-dependent manner of GLUT2 expression regulation, a model explaining nutrient-related regulation of GLUT2 at transcriptional and posttranscriptional levels was proposed by Ohtsubo (Figure 5). In normal metabolic conditions, SAPK2 phosphorylates PDX1, and SREBP-1c interacts with the transcriptional factors, leading to nuclear translocation and increased expression of GLUT2 (Ohtsubo et al., 2011). After synthesis, the N-glycosylation of GLUT2 occurs in the Golgi apparatus by glycosyltransferase Gnt4a, which allows further interaction with galectin 9 and anchoring on the cell membrane. In the case of imbalanced metabolism caused by a high-fat diet, the increased amount of free fatty acids inhibits the translocation of essential transcription factors, and synthesized GLUT2 is not glycosylated which leads to further lysosomal degradation (Ohtsubo et al., 2005, 20). Also, a dysfunction of GLUT2, which is essential in β-cell glucose uptake, leads to an alteration of insulin secretion.

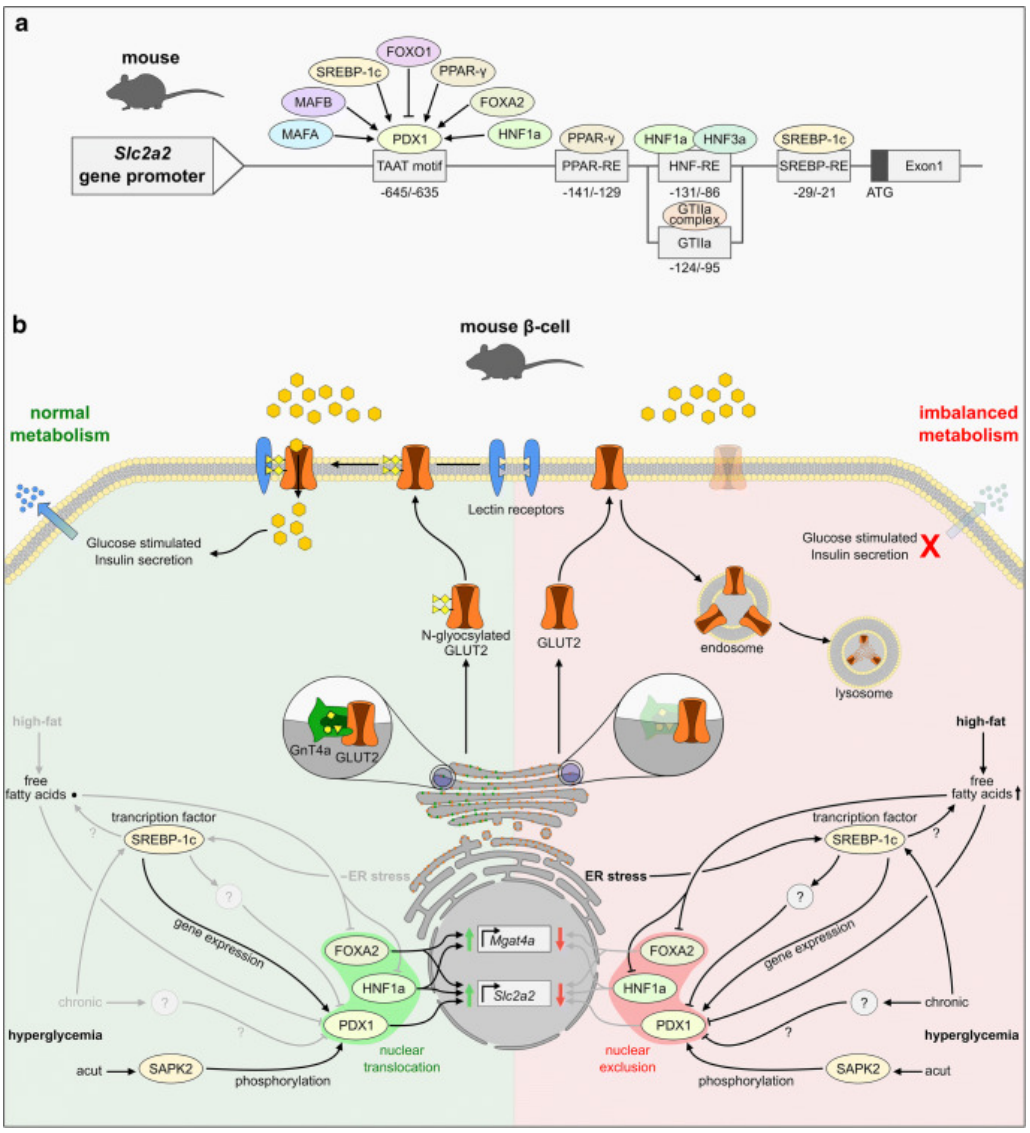

Figure 5: Nutrient-related regulation of *Slc2a2* gene expression and further aftermath of GLUT2: the green side of the cell indicates the normal pathway of GLUT2 caused by normal metabolism, while the red part of the cell shows the imbalanced metabolism with a high-fat diet leading to the internalization and degradation of GLUT2. It has been shown that the high-fat diet in mice disrupts O-glycosylation of GLUT2 and prevents further tethering to the membrane with galectin 9. Unglycosylated GLUTs are degraded by endosomes (Ohtsubo et al., 2011)

1.3. The cytoskeleton

Cytoskeleton represents a group of proteins that allow a single cell to adapt its shape in response to its surroundings and environmental impact. The adaptation of the shape is achieved by both assembling and disassembling the components of the cytoskeleton. Three major groups of the cytoskeleton are microfilaments, microtubules, and intermediate filaments. The groups differ not only in their chemical properties but also in the structures they form (Hohmann and Dehghani, 2019). The functional F-actin is formed after G-actin monomeric units are assembled. Actin filaments are known to generate force for movement and to change the shape of the cell. Microtubules are formed by α- and β-tubulin monomeric units which form protofilaments that are organized into ring structures. The role of microtubules is seen in facilitating intracellular transport,

formation of the mitotic spindle, and controlling the shape of the cell. Intermediate filaments are organized into larger filamentous units by aggregation of the monomer in a "coiled-coil" manner and these dimers are further assembled into tetramers. Eight tetramers are further assembled into a filament.

1.3.1. Intermediate filaments

Intermediate filaments (IFs) present a cytoskeletal network and provide structural support within the cell. They are found in eukaryotic cells and are comprised of over 70 various proteins that can be categorized into eight distinct families, based on their sequence and structure (Hol and Etienne-Manneville, 2015). In comparison to other types of cytoskeleton, IFs are organism-, organ-, and differentiation-specific cytoskeleton structures (Block et al., 2015). It has been shown that even though the difference in amino acid sequence exists between the intermediate filament proteins, common structural motifs can be seen within proteins, characterized by the presence of an N-terminal head, α-helical rod domain, and C-terminal tail (Chernyatina et al., 2015). The α-helical rod domain is built of three coil-shaped domains that are separated by linker domains, while the head and tail domains have variable structures (Nishimura et al., 2019). The point mutations that occur in the beginning and end parts of the helical rod domain strongly alter the physical properties of IFs and the dynamics of polymerization are affected (Etienne-Manneville, 2018). IFs are characterized by high structural stability and thus they are important for maintaining the shape and integrity of the cell and providing a scaffold for other organelles. IFs form dense meshwork in cells and the structure of these assemblies is determined by the type of IFs which are included in the formation. Five types of IFs have been described according to their assembly properties and known examples include proteins, such as keratins (type I and type II), vimentin and desmin (type III), neurofilaments (type IV), and nuclear lamins (type V) (Block et al., 2015; Etienne-Manneville, 2018). The classification of IFs into types reflects their function and their origin. The proteins of the IFs have a wide variety of functions, such as providing structural support, participating in cell signaling pathways, and helping to regulate gene expression. It has been shown that IFs have a large contribution to cell mechanics. The assembly of IFs does not need the assistance of co-factors (Herrmann et al., 2004). IFs are organized into bundles forming intracellular networks. These bundles comprise multiple filaments bound together by cross-links, which help stabilize the structure. The bundles are further assembled into structures, such as the nuclear lamina. The mechanism of IF assembly is explained by the binding of dimers, which in most cases are

homodimers, except for keratins, whose units form type I-type II heterodimers. Dimers are further assembled into tetramers and eight of them form a filament (Nishimura et al., 2019). The rod domain is responsible for this kind of assembly, as it interacts with other monomers and further tetramers. The assembly of IFs is nucleotide-independent, which means that no ATP or GTP is required, while the nucleotides are present in the assembly processes for actin filaments and microtubules. The assembly process is backed up by several principles: alignment of dimers is exact as in filaments, and the growth is dependent on the interaction between IF dimers (Chernyatina et al., 2015). One of the important features of IFs is self-assembly. For example, under chaotropic conditions, IFs showed the ability to self-assemble into filaments. tetrameric complexes of IF proteins are formed by joining two dimers in an anti-parallel manner, furthermore, tetrameric complexes form larger assembles under specific ionic strength conditions (Herrmann and Aebi, 2016). When the parameters of the solutions are adjusted *in vitro*, IFs self-assemble too.

IFs also help to form a scaffold that can anchor organelles, such as the nucleus, centrioles, and endoplasmic reticulum, to the cytoskeleton (Styers et al., 2005; Toivola et al., 2005). IFs also help to regulate gene expression by recruiting chromatin-modifying proteins to certain locations in the nucleus, which can affect gene expression. To perform their function, IFs interact with other organelles and nuclei via IF-associated proteins, which are also known for their roles in cell signaling and other physiological processes. Along with their known mechanical role, IFs are also found essential for organizing the space within the cell and maintenance during dynamic behavior. These roles include nucleus positioning, mitochondrial structure, localization, and membrane trafficking (Nishimura et al., 2019). IFs are known to interact with mitochondria and control their distribution, for instance, to anchor them in the vicinity of sites that demand high energy levels (Nishimura et al., 2019). Upon exposure to extracellular signals, a signaling cascade occurs and the expression of IFs is influenced. This includes interactions with IF-associated proteins and reorganization of the IF network. During stress, the levels of IFs increase, for example, in chronic diseases, IF proteins are overexpressed and aggregates are formed (Pekny and Lane, 2007; Toivola et al., 2010). It is assumed that the phosphorylation of IFs and reorganization of filaments are important for IFs to perform a protective role. In conclusion, IFs are important proteins that provide structural stability and support for the cell.

1.3.2. Keratins

Keratins (K) are known for their generally big molecular diversity, which is explained by genes required for their expression (Moll et al., 2008). In the human body, they are mostly expressed in epithelial tissues, hair, skin, and appendages. Keratins are expressed by 54 genes and they are classified into two groups: acidic type I (K9-K40) and neutral type II (K1-K8 and K71-86) (Etienne-Manneville, 2018). So far, 67 genes for keratin are described and 54 of them are functional. Within 54 keratin genes, 37 genes encode for keratins found in living cells, and 17 for keratins within the hair and nails (Herrmann and Aebi, 2016). Keratins are assembled by forming heterodimers consisting of type I and type II keratins. It is known that this kind of assembly leads to loose distribution within the cell and little bundling. A relevant characteristic of keratins is specific pairs of keratins are found in cell-specific and differentiation state-selective manner (Omary et al., 2009). Their further polymerization is regulated by phosphorylation, O-glycosylation, sumoylation, ubiquitination, and acetylation (Etienne-Manneville, 2018). These post-translational modifications allow keratins to regulate assembly, disassembly, structural integrity, and cellular metabolism: for example, the phosphorylation of K8 allows change of the solubility and filament assembly. Similarly, the sumoylation of keratins is observed when oxidative or apoptotic stress occurs, while the glycosylation of K18 provides protection from injury (Snider and Omary, 2014). The structure of keratins can be explained by the presence of three distinct regions: N-terminal head, α- helical rod domain, and C-terminal tail (Figure 6). The N-terminal head domain contains up to 100 amino acids and is known for interactions with other molecules, while the tail domain is globular and is crucial for the keratin diameter (Herrmann and Aebi, 2016). The tail domain is known for the *in vitro* stabilization of keratins. The helical rod domain is a central and conserved part of keratins. Helical segments of the rod domain are connected by linker domains L1, L12, and L2 (Toivola et al., 2015). Keratins generally provide mechanical stability but are also crucial for adapting and responding to the cellular environment.

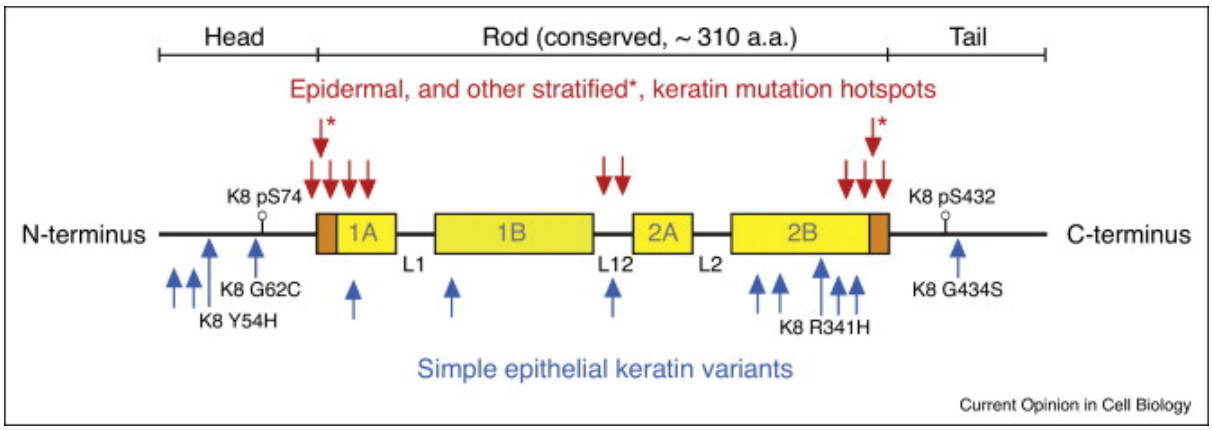

Figure 6: Simplified overview of keratin domains and their mutational hotspots (Toivola et al., 2015)

The function of keratins is determined by the type of keratins and organ/cell where keratins are expressed (Alam et al., 2013; Pan et al., 2013). Keratins are also divided according to their distribution in organs, and therefore several types of keratins can be distinguished: hair keratins, epidermal, and simple epithelial keratins (Strnad et al., 2016). Within organs, simple epithelial keratins can be assembled in a cell-specific manner or in layers, which explains their variation in organs and functions. The importance of keratins in human physiology has been emphasized by the presence of more than 80 keratin-related human diseases. Mutations within keratin proteins occur at the hotspots within the rod domain and these mutations can cause cells and tissues to deteriorate, as they become more fragile (Toivola et al., 2015). Keratins also provide protection from cell death when they get glycosylated: the glycosylation of K18 leads to the phosphorylation of Akt at residue 308, which further inhibits cell death (Ku et al., 2010). The desmosome-keratin system, which involves the activity of desmoplakin, is necessary for the stability of epithelial tissues (Gross et al., 2022).

In the head and tail domains, post-translational modifications and phosphorylation occur. The inherited alteration, malignant transformation, and non-neoplastic diseases cause variations within keratin architecture which include filament reorganization, altered solubility, and mechanical fragility (Toivola et al., 2015). Due to the retention of their properties during tumor differentiation, keratins can be used as important markers in diagnosis and tumor classification. K5-K8 and K18-20 have been known for their use as clinical markers in pathology. It has been shown that stress and disease conditions lead to keratin upregulation in organs, such as the pancreas, colon, liver, and kidney (Alam et al., 2018).

1.3.2.1. Keratins in the endocrine pancreas

The most important keratins in the endocrine pancreas include K8 and K18. Alam and colleagues showed that the absence of K8 in pancreatic β-cells affects insulin control and their ultrastructure: the morphology of insulin vesicles is disrupted and altered compared to the wild-type mice (Alam et al., 2013). Another important factor for the function of keratins in the physiology of β-cells is that the structure and activity of mitochondria are suggested to be controlled by keratins via trichoplein-mitofusin interactions, as keratins bond to mitofusin protein via trichoplein (Silvander et al., 2017). The global knockout of K8 in mice leads to the alteration of β-cell mitochondrial morphology in terms of a decrease in size and increased fragmentation: keratins are essential for maintaining both mitochondrial membrane potential and ATP production. For functional and proper insulin production, adequate ATP production is required. Keratins are suggested to be needed for maintaining a normal morphology of insulin vesicles and membranous localization of glucose transporters: the global knockout of keratins in mice shows more intracellular distribution of GLUT2 and lower glucose uptake in β-cells. In streptozotocin (STZ)-induced diabetic and non-obese diabetic mice, keratins, especially K8, were upregulated and this was significant for protection from diabetic stress or injury (Alam et al., 2013). On the other hand, the K8-knockout mice have lower islet damage and this can explain the possibility of protection from STZ-induced injury due to the mislocalization of GLUT2. It has been shown that along with K8 and K18 in islets of Langerhans, K7 is present, however, the absence of K8 leads to the downregulation of both K7 and K18, (Alam et al., 2021). It has been confirmed that the levels of K7 increase during diabetes-caused stress in the vicinity of the nucleus, indicating that K7 with other keratins can play an important role in β-cell physiology and recovery (Alam et al., 2021). The roles of keratins in β-cells are summarized in the figure below (Figure 7).

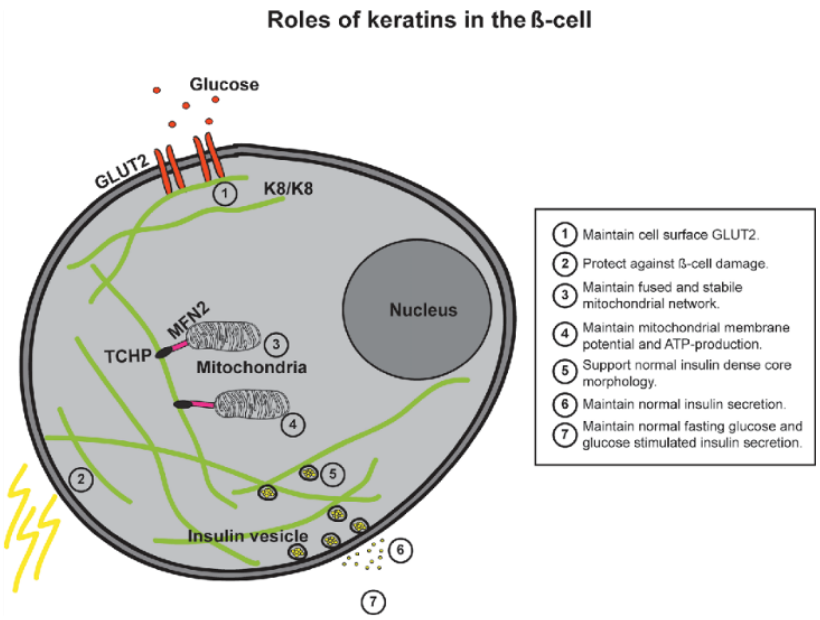

Figure 7: Summarized roles of keratin in β-cells (Silvander et al., 2017)

1.4. Cre-loxP system in generating conditional knockout mice

To examine the gene functions in various cells and tissues, the Cre-loxP system has been implemented and is well-known in biomedical research. The Cre-loxP system requires two elements to be successfully achieved. Firstly, an animal must carry a locus that is flanked by two loxP motifs with the length of 34 base pairs (two 13 bp inverted and palindromic repeats and 8 bp core sequences) and cells should express a Cre recombinase enzyme (McLellan et al., 2017). Gene or a DNA segment can be generated when working with embryonic stem cells and further transplanted into a murine blastocyst. Cre recombinase enzyme is characterized by its specificity and many promoters or enhancers are used to drive the expression of Cre in the tissue of interest (McLellan et al., 2017; Kim et al., 2018). To assess the role of keratins in ß-cells, the Cre-loxP system is used to generate mice that lack keratin 8 in β-cells (Figure 8). For instance, the *KRT8* gene was flanked by loxP sequences, and the activity of Cre recombinase was assisted by the promoter insulin to disable the expression of K8 in β-cells.

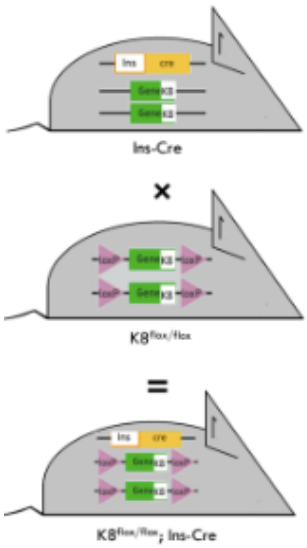

Figure 8: A simplified figure shows mice with the genotypes: Ins-Cre mice express Cre recombinase with insulin as a promoter, while $K8^{flox/flox}$ mice have the K8 gene flanked between loxP sequences. After breeding genotypically different mice, a new strain is formed lacking keratin 8 in β-cells

Although the Cre-loxP system is widely used in research, there are limitations that scientists should consider when working. For example, a possibility of potential off-target Cre expression exists which may confuse when obtaining the final data. Along with off-target expression, toxicity has been reported very often as a common limitation: mammalian cell proliferation was reduced and chromosomal defects were observable (McLellan et al., 2017). Other limitations include the excision of loci and reduced cell and tissue specificity. Regardless of the limitations and challenges that the Cre-loxP system faces, this approach is a promising and established method that helps elucidate the roles of genes in cells and tissues.

2. Aims and hypotheses

Keratins are one of the most significant intermediate filaments regarding the physiology and mechanobiology of epithelial cells, due to their properties and interactions with other proteins. Previous work and publications emphasized the importance of keratins in β-cell function and during diabetic stress. With everything stated in the literature review and focusing on the role of keratins in T1D, three aims have been hypothesized for the thesis work.

Aim 1: To investigate if K8 is involved in the regulation of β-cell proliferation. The hypothesis is based on the preliminary data on histology analysis demonstrating an increase in the size of islets in conditional β-cell-specific K8 knockout mice compared to the control.

Aim 2: To investigate the role of β-cell K8 in cell stress protection upon exposure to streptozotocin in islet β-cells of β-cell-specific K8 knockout. The hypothesis is that islets of conditional β-cell-specific K8 knockout mice are less susceptible to streptozotocin-induced cell damage This hypothesis is supported by the previous publication using global knockout of K8 in mice showing less damaged islets compared to control mice.

Aim 3: To investigate the role of β-cell K8 in GLUT2 plasma membrane targeting. The hypothesis is that the absence of K8 in β-cells of conditional β-cell-specific K8 knockout mice leads to GLUT2 membrane mislocalization.

3. Materials and Methods

3.1. Mice. $K8^{flox/flox}$ transgenic mice in the C57BL/6 background (Stenvall et al., 2022) were used to generate a β-cell-specific K8 knockout mice. $K8^{flox/flox}$ were bred with female $Ins1^{Cre}$ mice (Thorens et al., 2015) (from JAX stock #026801) and the conditional mice were maintained by breeding $K8^{flox/flox}$ with $K8^{flox/flox}$; Ins-Cre. As a secondary control for all the mouse experiments, $Ins1^{Cre}$ mice were used which were maintained by breeding female $Ins1^{Cre}$ mice with male $K8^{flox/-}$ (here Cre^{-}). Mice were genotyped as described previously (Stenvall et al., 2022). All mice were housed at the Central Animal Laboratory at the University of Turku and handled according to the animal study licenses 197/04.10.07/2013, 3956/04.10.07/2016 and ESAVI/16359/2019, approved by the State Provincial Office of South Finland. Male age-matched mice (2-6 months and 18 months old) were used throughout this study. For the STZ treatment, a solution was prepared in 50 mM sodium citrate in PBS (pH 4.5). STZ solution was administered to mice intraperitonally in a single dose of 140 $\frac{mg}{kg}$ After the experiments, mice were killed by CO_2 asphyxiation and the pancreata were collected for the sample preparation.

3.2. Histological analysis. Microscopic slides of the H&E-stained and Masson-Trichrome-stained murine pancreas were scanned and images were acquired using Pannoramic 1000 device (3DHistech Kft, Hungary) at Medisiina Imaging Centre of the University of Turku, Finland. Each microscopic slide contains four sections from the same mouse. Images were saved as .mrxs files to process them further with the QuPath software (Bankhead et al., 2017). From every image, two sections were chosen and islets and their representative sections were annotated with Brush and Wand tools. Islets were counted for every annotated section and the damage score was assessed according to the scale 0-4: 0 – no damage; 1 – up to 10% damage; 2 - up to 30% damage; 3-up to 50% damage; 4 – more than 50% damage (Figure 9). A number of islets with the corresponding score was moved to an Excel file. The values that correspond to the area of islets (islet size) and sections were exported. Islet mass was calculated by dividing the islet area by the section area and multiplying it by 1 000 000. In images regarding basal histology of untreated mice, islets were annotated and the Cell Detection option in QuPath software

was run to detect the nuclei within the islet. 3 islets from every mouse were analyzed and sections from 3 mice from every genotype were used. Analysis of basal histology was done in three groups: the first group considered islets regardless of the size, then the second group consisted of islets with a size between 5000 and 14000 μm^2, and the final group consisted of islets bigger than 14000 μm^2. Masson-Trichrome staining was performed at the Histology core facility of the University of Turku for collagen staining.

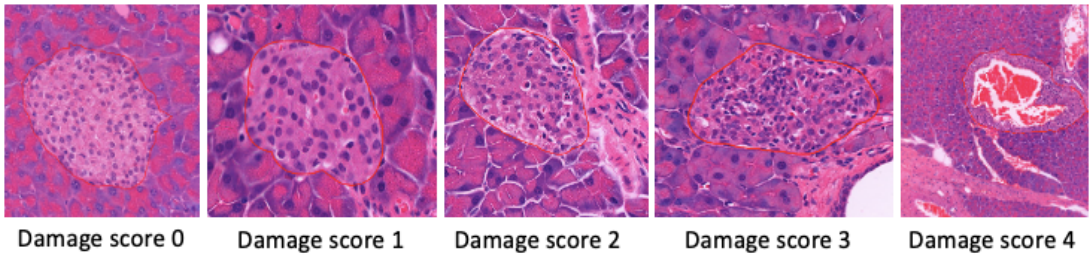

Figure 9: A scale from 0 to 4 was set up for the islet damage score assessment after STZ exposure: 0 – no damage; 1 – up to 10% damage; 2 – up to 30% damage; 3 – up to 50% damage; 4 – more than 50% damage. Examples of the islets with every assigned representative score are shown here.

3.3. Sample preparation. Frozen OCT pancreas tissue samples of $K8^{flox/flox}$ and $K8^{flox/flox}$; Ins-Cre mice were sectioned using CM3050 Leica Cryostat. Samples were trimmed and sectioned with a thickness of 6-7 µm for further stainings for proteins and structures of interest. Two fixation methods were used: acetone fixation and 1% paraformaldehyde (PFA) fixation.

3.4. Immunofluorescence staining**.** Primary antibody solutions were made in required ratios and upon adding, the samples were stored for overnight at 4ºC. Fluorescently labeled secondary antibodies recognizing the immunoglobulin of the first antibody were incubated for 45 minutes. Antigens studied were insulin, GLUT2, E-cadherin, Ki67, β-catenin, and YAP. Primary antibodies used were; guinea pig anti-insulin (Progen, Heidelberg, Germany), rabbit anti-GLUT2 (Merck Millipore, Temecula, CA, USA), rat anti-E-cadherin (Invitrogen, Eugene, OR, USA), rabbit anti-Ki67 (Abcam, Cambridge, UK), rabbit anti-β-catenin (Abcam, Cambridge, UK), and rabbit anti-YAP (Cell Signaling Technologies, Danvers, MA, USA) and mouse anti-desmoplakin (kind gift from Eriksson lab, Åbo Akademi University, Finland). Secondary antibodies used were goat anti-guinea pig Alexa 546, donkey anti-rat Alexa 568, and donkey anti-rabbit Alexa 488 (Invitrogen, Eugene, OR, USA).

3.5. Antibodies. Antibodies were used for staining and labeling molecules of interest. The tables of primary and secondary antibodies used are shown below (Tables 1 and 2).

Table 1. The list of primary antibodies used for staining of pancreatic sections. Target antigen, host, ratio, and producer are listed

Target antigen	Host	Ratio used	Producer
insulin	guinea pig	1:1000	Progen
GLUT2	rabbit	1:200	Merck
E-cadherin	rat	1:200	Invitrogen
Ki67	rabbit	1:200	Abcam
β-catenin	rabbit	1:250	Abcam
YAP	rabbit	1:200	Cell Signalling Technologies
desmoplakin	mouse	1:50	Eriksson lab

Table 2. The list of secondary antibodies used for targeting primary antibodies. The name, ratio used, and producer are listed below

Secondary antibody	Ratio used	Producer
goat anti guinea pig 546	1:200	Invitrogen
donkey anti rat 568	1:200	Invitrogen
donkey anti rabbit 488	1:200	Invitrogen

3.6. Imaging. Stained samples were imaged using a 3i spinning disk confocal microscope. Objectives used were 63x and 100x. Exposure times for every channel were 200 ms for 405 nm, 100 ms for 488 nm, and 200 ms for 561 nm, regarding the GLUT2 analysis. For other molecules, only the time for 488 nm differed, which was 500 ms. For E-cadherin, an adjustment was made, and the exposure time for the 561 nm laser was 400 ms. After the image acquisition and adjustments (for $K8^{flox/flox}$ and $K8^{flox/flox}$; Ins-Cre) for GLUT2 and K8 using ImageJ, peak fluorescence intensity was measured using the quantification approach: a line for the region of interest was drawn between the nuclei of two neighbouring β-cells. The fluorescence intensity for the proteins was measured

along the drawn line. The optical plane was chosen with the larger diameter of the nuclei. The GLUT2 analysis is facilitated by co-staining of membrane markers (E-cadherin) and this further demonstrates the colocalization of GLUT2 and the marker of interest. YAP nuclear localization was measured by calculating the area of the region of interest which corresponds to the nucleus of the cells, characterized by a stronger signal of YAP.

3.7. Statistical analysis. Statistical analytical tests were run to assess relevant parameters: one-way ANOVA and t-test. For one-way ANOVA, multiple comparisons were run and the means of every group between each other were compared. For assessing the most common values of the parameters, frequency distribution was performed and shown as a percentage. Statistical analysis was done using GraphPad Prism software.

4. Results

4.1. Histological analysis of untreated mice

4.1.1. Mice that lack K8 in β-cells have bigger islets than wild type $K8^{flox/flox}$ mice

In order to investigate if the loss of β-cell K8 leads to a histological change in the endocrine pancreas, cell size, nucleus size, and cell number were analyzed. Cell size was determined by dividing the islet area by the number of nuclei. The results show that there is no difference in cell size and nucleus size between the islets from the wild type ($K8^{flox/flox}$) and conditional knockout ($K8^{flox/flox}$; Ins-Cre) mice. The preliminary data from the basal histology analysis showed that the knockout mice had a higher number of large-sized islets (Figure 10A). Therefore, to investigate basal histology and its related parameters, we divided our data into two groups: the first group included islets with a size between 5000 and 14000 μm^2 (Figure 10B), while the other included islets with a size bigger than 14000 μm^2. The threshold for the data grouping was based on the islet size distribution graph from preliminary work. The graph shows that most of the β-cell K8 knockout islets are bigger than 14000 μm^2 (Figure 10A). After obtaining the preliminary results, 4 biggest islets bigger than 14000 μm^2 were analyzed. It was found that bigger cells are found in the islets of $K8^{flox/flox}$; Ins-Cre (Figure 10C) and this led to further work regarding proliferation and collagen content in the extracellular matrix, which is explained in section 4.2.

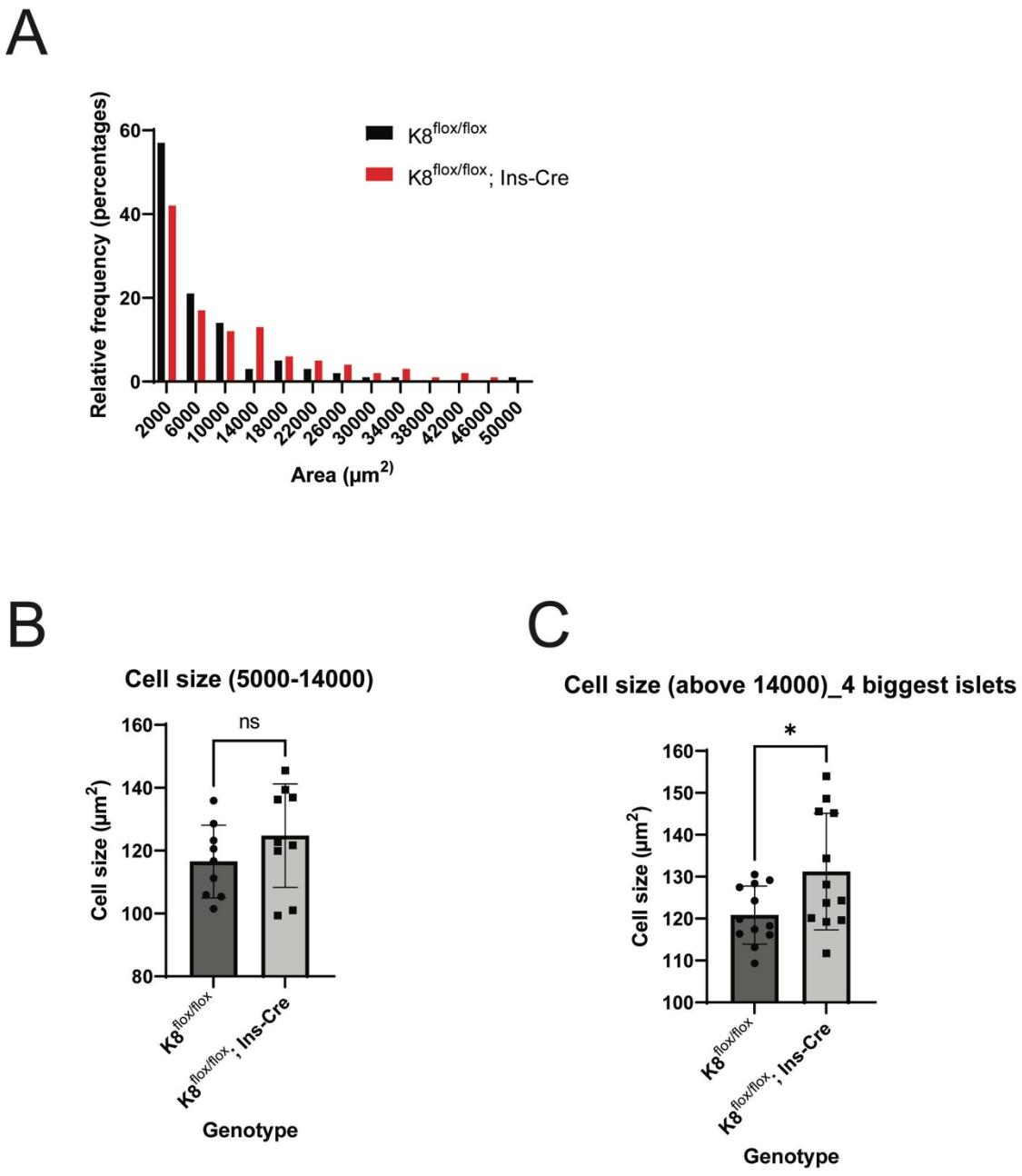

Figure 10: More large-sized islets are found in K8$^{flox/flox}$; Ins-Cre mice compared to K8$^{flox/flox}$ mice. The threshold for two separate analyses was put at 14000 µm^2 because the islets bigger than the threshold value are found more in conditional knockout mice (A); the cell size does not differ between K8$^{flox/flox}$ and K8$^{flox/flox}$; Ins-Cre mice in smaller islets (B); the biggest islets of K8$^{flox/flox}$; Ins-Cre mice are characterized with bigger cells compared to K8$^{flox/flox}$ mice (C). n refers to the number of islets: (B) n=9 and (C) n=12. p-value: * (<0.05).

4.1.2. The nucleus size between K8$^{flox/flox}$ and K8$^{flox/flox}$;Ins-Cre mice does not differ

It was hypothesized that bigger nuclei appear in the islets of conditional knockout mice due to mechanical stress. (Figures 11A and 11B). The nucleus size remains the same between K8$^{flox/flox}$ and K8$^{flox/flox}$; Ins-Cre regardless of the islet area.

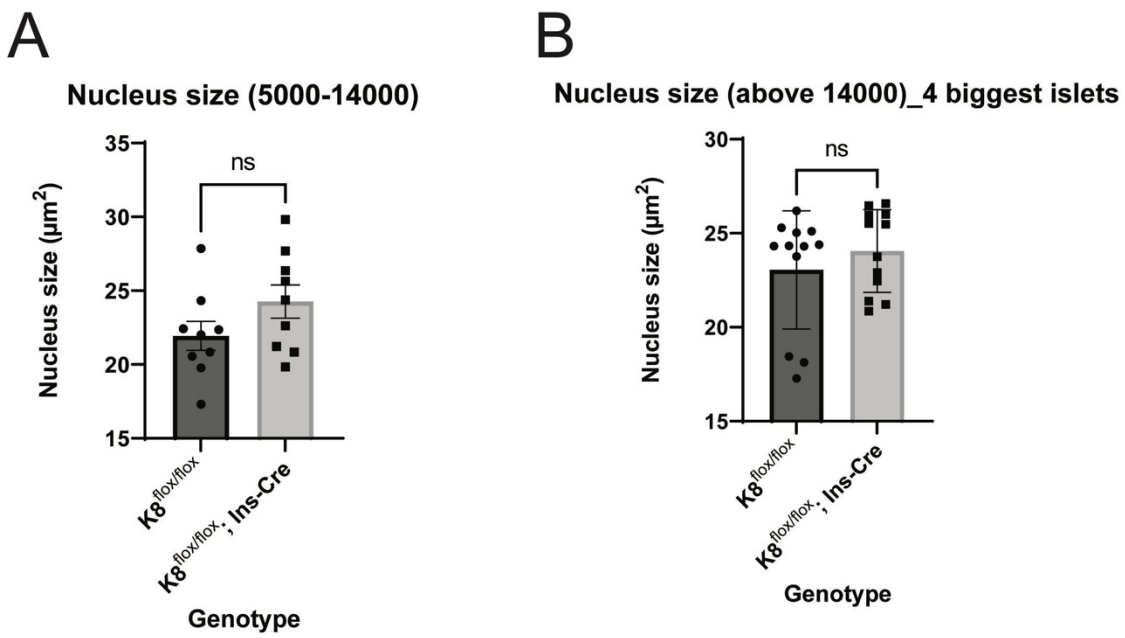

Figure 11: The nuclei of both K8$^{flox/flox}$ and K8$^{flox/flox}$; Ins-Cre do not differ in size. Histological analysis using QuPath showed that the presence or absence of keratins does not affect the properties of the nuclei. Nucleus size was shown for both smaller (A) and larger islets (B). No significant (ns) difference is seen in both groups between the genotypes. Three biggest islets from every mouse were used in A (n=9), while in B four biggest islets were analyzed (n=12). Three mice have been used per genotype (K8$^{flox/flox}$ and K8$^{flox/flox}$; Ins-Cre).

4.1.3. Cell number in islets between K8$^{flox/flox}$ and K8$^{flox/flox}$; Ins-Cre shows no difference

Histological analysis of pancreatic islets showed no significant difference of the cell number between K8$^{flox/flox}$ and K8$^{flox/flox}$; Ins-Cre mice (Figures 12A and 12B).

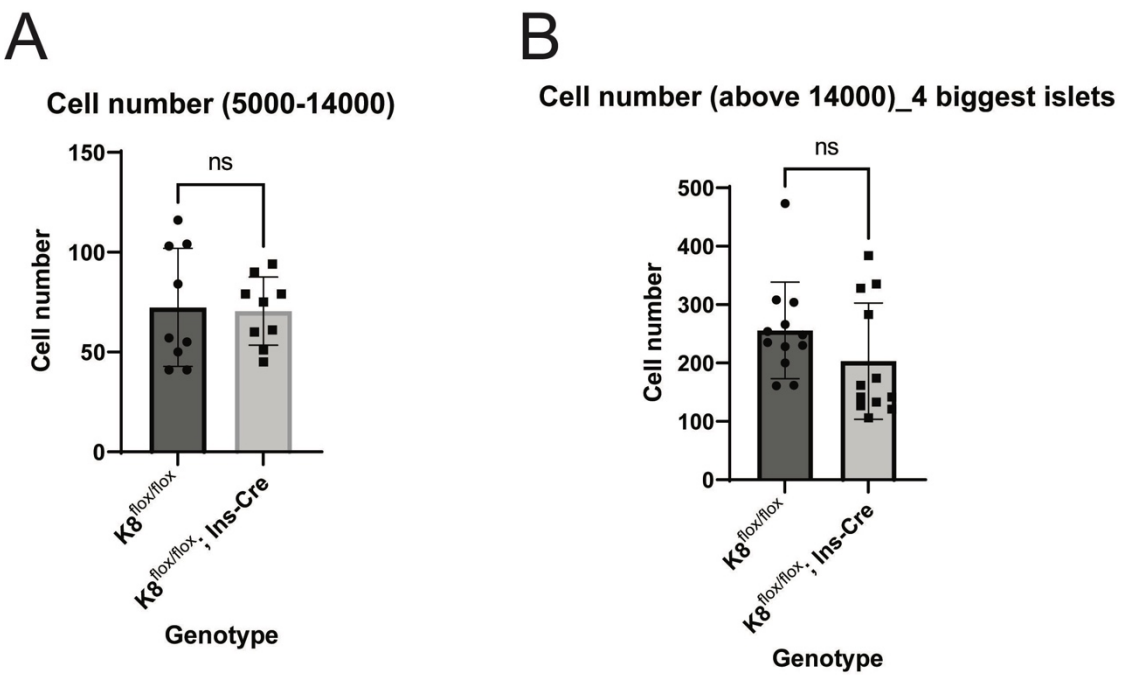

Figure 12: Cell number remains the same in the islets of conditional knockout mice and the wild-type mice. It was hypothesized that the cell number might contributed to the bigger size of islets in $K8^{flox/flox}$; Ins-Cre The cell number does not differ between $K8^{flox/flox}$ and $K8^{flox/flox}$; Ins-Cre for both categories: smaller islets (A) and bigger islets (B). Three biggest islets from every mouse were used in A (n=9), while in B four biggest islets were analyzed (n=12). Three mice have been used per genotype ($K8^{flox/flox}$ and $K8^{flox/flox}$; Ins-Cre).

4.2. Proliferation of β-cells

4.2.1. The increase in the islet size in $K8^{flox/flox}$; Ins-Cre is not related to an increase in β-cell active proliferation in adult mice

Ki67 was used as a proliferation marker to analyze if keratins affect the proliferation within pancreatic islets which could contribute to the increased islet size. After analyzing images (representative images are shown in Figure 13A) with a detectable signal of Ki67 within the islet, it can be concluded that no major proliferation occurs within the endocrine pancreas and no difference in Ki67 signal between $K8^{flox/flox}$ and $K8^{flox/flox}$;Ins-Cre mice (Figure 13B).

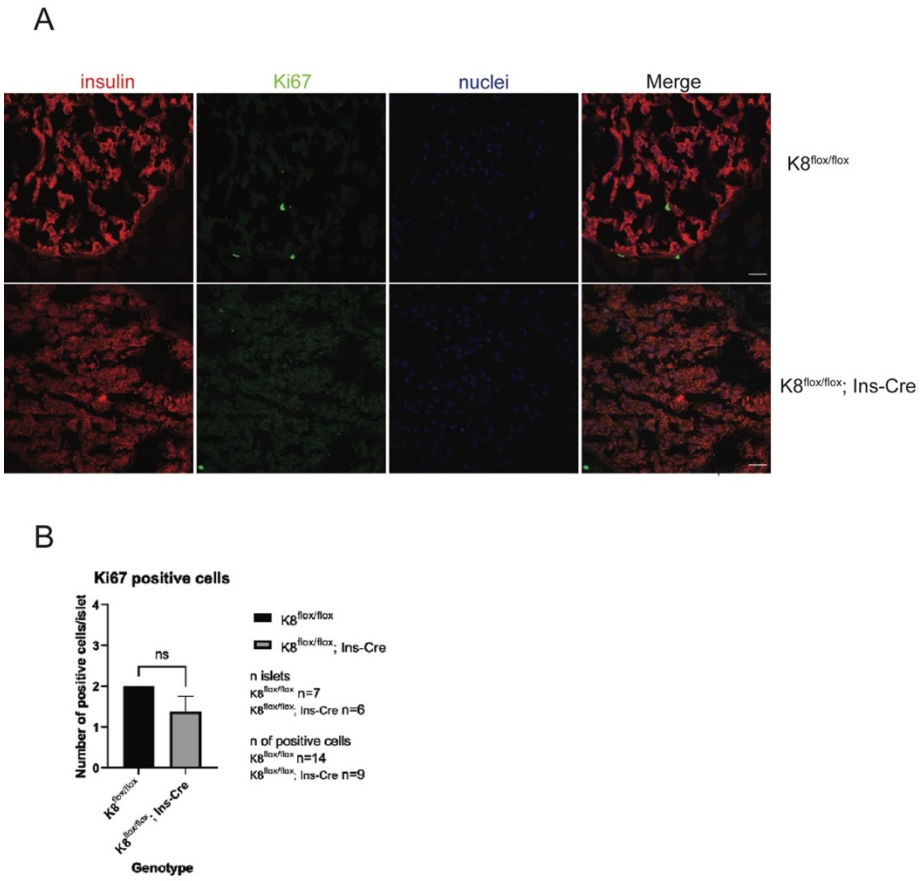

Figure 13: The number of Ki-67 positive cells in pancreatic islets does not indicate changes in beta cell proliferation after cell-specific K8 deletion**.** Multichannel images show islets after staining for insulin (red) and Ki67 (green). The few observable Ki67-positive cells are found peripherally of the islet (A). Scale bar: 20 µm. The graph below shows no significant (ns) difference between $K8^{flox/flox}$ and $K8^{flox/flox}$; Ins-Cre mice (B). Number of islets: n=7 for $K8^{flox/flox}$ and n=6 for $K8^{flox/flox}$; Ins-Cre.

4.2.2. YAP nuclear localization does not initiate the proliferation in pancreatic β-cells of $K8^{flox/flox}$ and $K8^{flox/flox}$; Ins-Cre mice

It is known that Yes-associated protein (YAP) is involved in the Hippo signalling pathway and can lead to proliferation if catenins are inhibited (Uttagomol et al., 2019). YAP is also used to study if the tissues and cells are mechanically compromised due to an increase in cell size. Therefore, YAP staining was used to analyze if a change occurs after the deletion of K8 in β-cells (Figure 14A), but after quantifying the images, no difference in YAP expression was seen in $K8^{flox/flox}$ and $K8^{flox/flox}$; Ins-Cre mice (Figure 14B). It was expected that more YAP signals would be observed in $K8^{flox/flox}$; Ins-Cre compared to $K8^{flox/flox}$ mice. The p-value though not significant (p=0.09) was close to the margin of 0.05, going in the direction that $K8^{flox/flox;}$; Ins-Cre mice might have proliferation-related size increase. With everything stated, it might be considered to do another imaging session for YAP using pancreas sections from more mice.

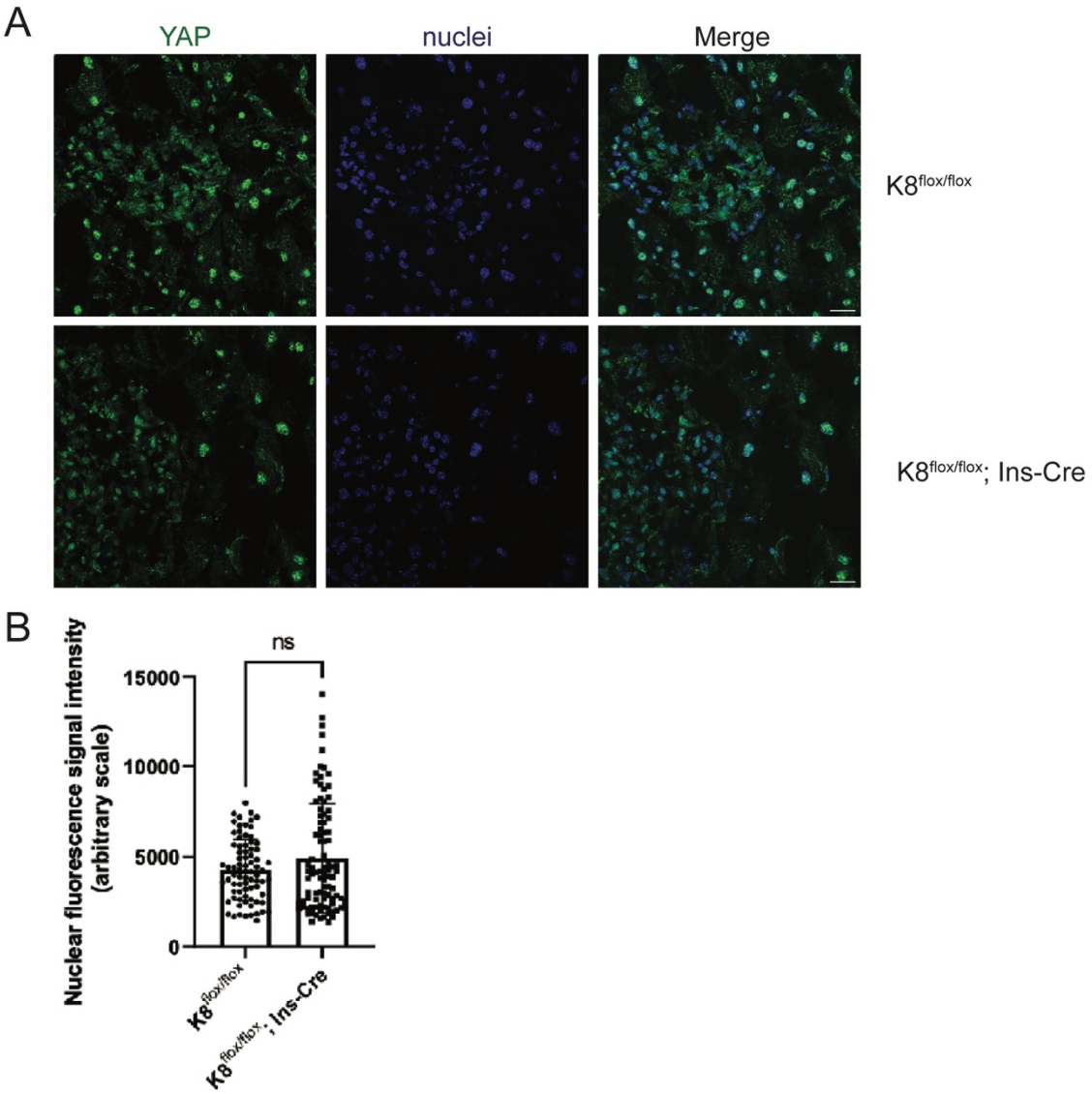

Figure 14: Even though the trend for nuclear localization of YAP in conditional knockout mice follows, no difference occurs. Multichannel images of YAP (green) and nuclei (blue) to show the localization of YAP between the control (upper row) and conditional knockout (lower row) (A). Scale bar: 20 μm. Graph (B) shows the nuclear localization based on the measurement of nuclear fluorescence signal intensity. Though it seems that YAP is more localized in the nuclei of knockout, there is no difference between the genotypes (P-value: 0.09).

4.2.3. Lack of K8 in β-cells does not lead to nuclear internalization of β-catenin

β-catenin was analyzed in order to investigate its expression and localization in β-cells, due to the bigger islet size in $K8^{flox/flox}$; Ins-Cre mice. β-catenin, which exerts its activity in the nucleus, is tethered on the cell membranes by E-cadherin, which decreases proliferation and inhibits Wnt signalling pathway (Wakae-Takada et al., 2013) The staining of pancreases from both genotypes showed no difference in the nuclear distribution of β-catenin. Overall, the clear signal of β-catenin was seen only within cell membranes (Figure 15).

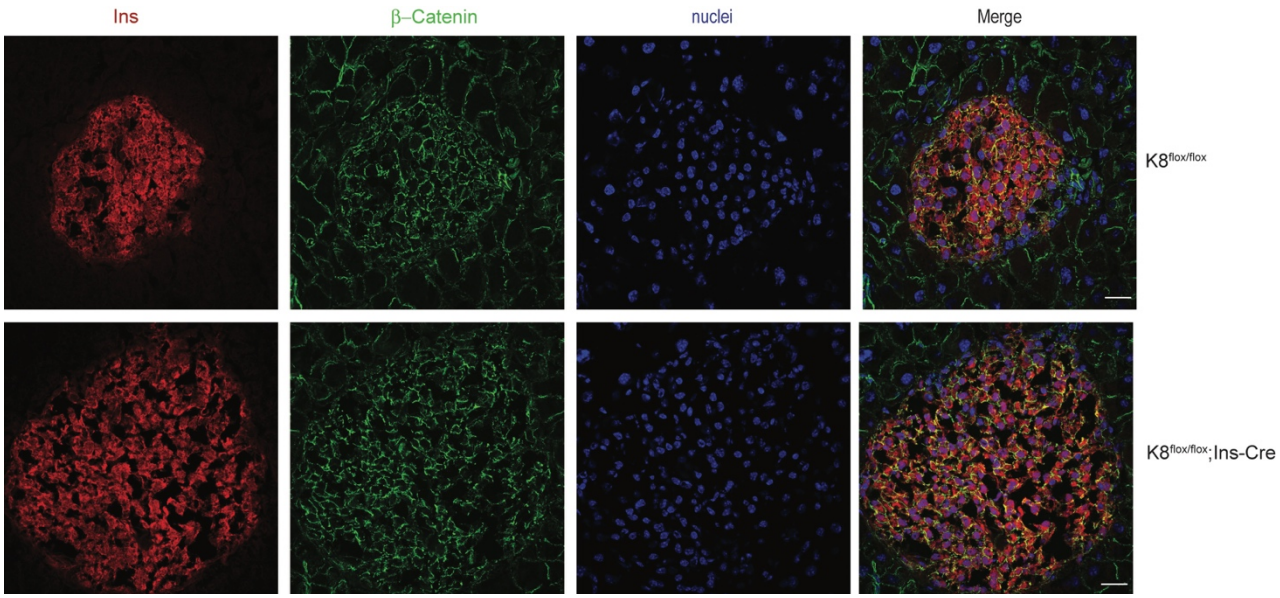

Figure 15: β-catenin is not internalized when K8 is knocked out from β-cells. Image comparison between $K8^{flox/flox}$ and $K8^{flox/flox}$; Ins-Cre mice after staining and imaging for insulin and β-catenin. No significant difference in nuclear distribution of β-catenin is seen between the genotypes. Scale bar: 20

4.2.4. Desmoplakin staining shows that the desmosomes of cell-cell contacts do not differ between $K8^{flox/flox}$ and $K8^{flox/flox}$; Ins-Cre mice

Desmoplakin was used for the assessment of the junctions and cell-cell contacts within the islet. The hypothesis was that desmoplakin is more compact in β-cell K8 knockout than in the wild-type mice. However, the staining and imaging for desmoplakin showed no difference in intensity and abundance of desmoplakin between $K8^{flox/flox}$ and $K8^{flox/flox}$; Ins-Cre mice (Figure 16).

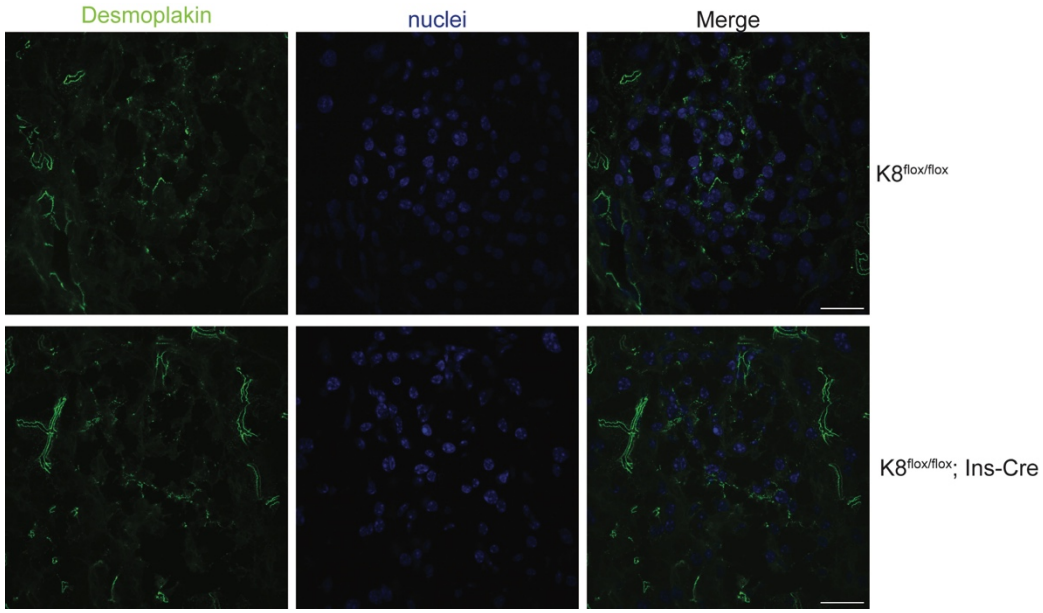

Figure 16: The knockout of K8 does not alter nor affect the cell-cell contact between neighboring β-cells. Image comparison between wild-type and knockout mice for desmoplakin. No difference in desmoplakin distribution within the islet is seen. Scale bar: 20 μm.

4.2.5. Collagen content does not contribute to the increase of islet size

The results of the proliferation-related analysis showed no significant difference between the K8 genotypes and the assumption for further work regarding the difference in islet size is collagen abundance and its distribution inside and around the islets. To investigate the underlying reasons for bigger islet size in $K8^{flox/flox}$;Ins-Cre mice, staining for collagen type I in the pancreatic islets was done. Masson-Trichrome staining was performed for staining collagen which is coloured blue (Figure 17A). After staining and quantifying the sections with islets, there was no significant difference (Figure 17B). It is also worth mentioning that most collagen in the pancreatic sections was seen around blood vessels and pancreatic ducts.

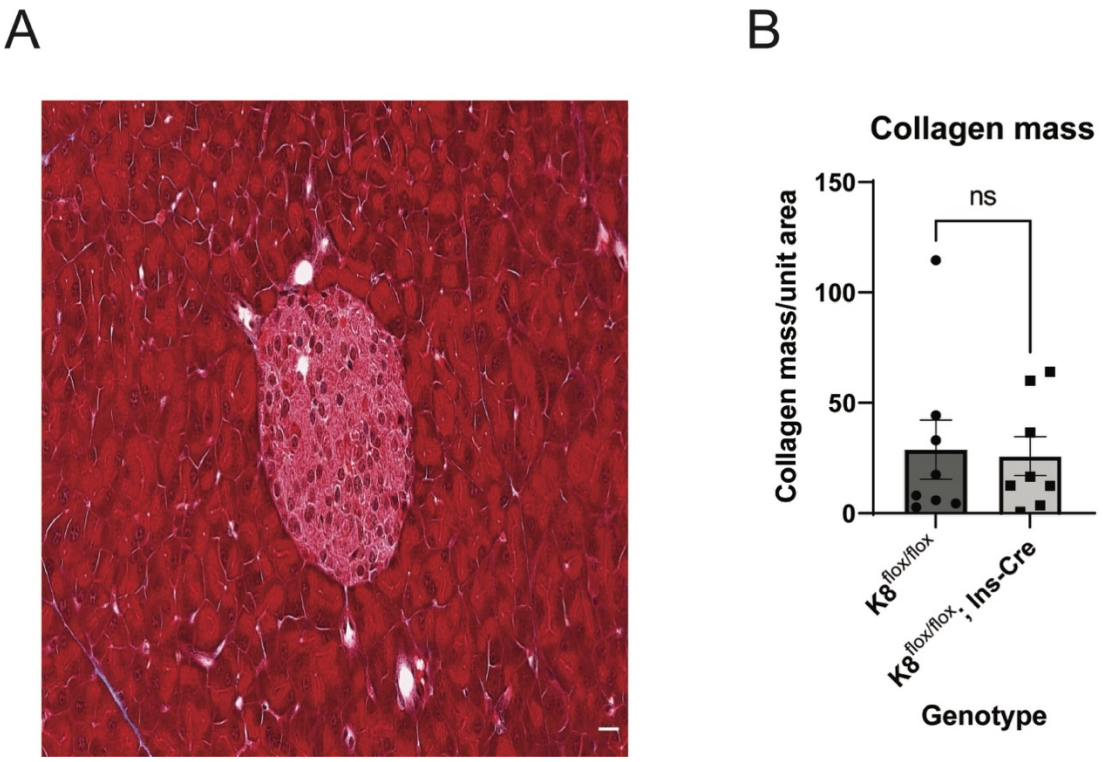

Figure 17: The collagen content in pancreatic islets is neglectable and does not differ between $K8^{flox/flox}$ and $K8^{flox/flox}$; Ins-Cre mice. Masson-Trichrome staining (A) showing islet, exocrine pancreas and collagen bundles (blue). It was observed that most of the collagen is found by the blood vessels and pancreatic ducts. Graph (B) shows no difference in collagen distribution in islets or their proximity.

4.3. Absence of β-cell keratins protects islets from streptozotocin exposure

4.3.1. Islets from $K8^{flox/flox}$; Ins-Cre mice are less susceptible to damage caused by streptozotocin

To investigate the role of β-cell keratins after diabetic stress, mice were treated with a high dose of streptozotocin (STZ) ($140\frac{mg}{kg}$) prior to the start of this thesis work. After the experiments, slides of the murine pancreas were stained with hematoxylin and eosin, then scanned, and the islet-relevant parameters damage score, islet size, islet mass, and islet number were assessed. Two datasets were used in the QuPath analysis: an image dataset from the high-dose streptozotocin done in November 2021 (here called experiment 1), and the other image dataset from an experiment conducted in June 2022 (experiment 2). The main finding observed after the STZ treatment and QuPath analysis is that the damage scores for controls ($K8^{flox/flox}$ and Cre^-) are higher than in conditional knockout ($K8^{flox/flox}$; Ins-Cre). Graphs for the islet damage are shown below for experiment 1, experiment 2, and both experiments combined (Figures 18A and 18B). The only difference in regards to controls from experiments 1 and 2 can be seen in a higher value of damage score for Cre^- mice from experiment 2 than the ones from experiment 1. However, another consideration for a slightly higher damage score in Cre^- can be also seen in the number of assessed islets: 114 islets were assessed from Cre^- mice used in experiment 1 compared to 62 islets assessed from the mice with the same genotype used in experiment 2 experiment.

Along with the assessment of islet damage score for all islets analyzed, a new assessment was done for islets with 50% damage and more (damage scores 3 and 4) (Figure 19). The graphs also show the damage score values for experiment 1, experiment 2, and both experiments combined (Figure 19). When it comes to the islets from mice used in experiment 1, the result shows that $K8^{flox/flox}$ mice have more islets with more than 50% damage (Figure 19A). On the other hand, the graph related to experiment 2 shows completely different values (Figure 19B): Cre^- mice have more islets with higher damage (≥50%) and this result can raise questions related to the physiology, phenotype, and possible related anomalies in Cre^- mice. Also, an attempt to see if there is a corresponding relation between glucose level and damage score was done, but no correlation was seen (Supplementary Figures 1 and 2).

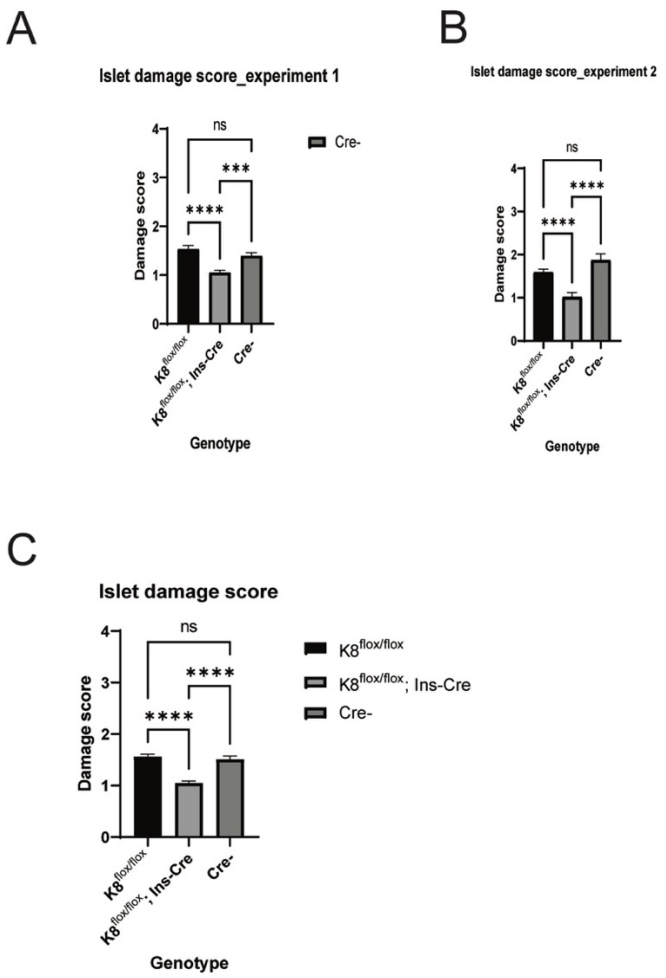

Figure 18: When exposed to streptozotocin, the islets of conditional knockout mice show lower damge and lower diabetes susceptibility. Conditional knockout mice are characterized with the islets that are less susceptible to diabetes and streptozotocin (STZ)-induced damage. The graph (A) shows the islet damage score for the mice used in experiment 1 and it is seen that conditional knockout mice have significantly lower damage score compared to both controls. A graph from experiment 2 (B) shows similar pattern as the experiment 1, with Cre^- mice and their islets being more susceptible and vulnerable upon diabetes and STZ exposure. The summary of both experiments is shown on the graph (C) emphasizing the effect of keratin absence upon the exposure to streptozotocin. p-values (***<0.001, ****<0.0001)

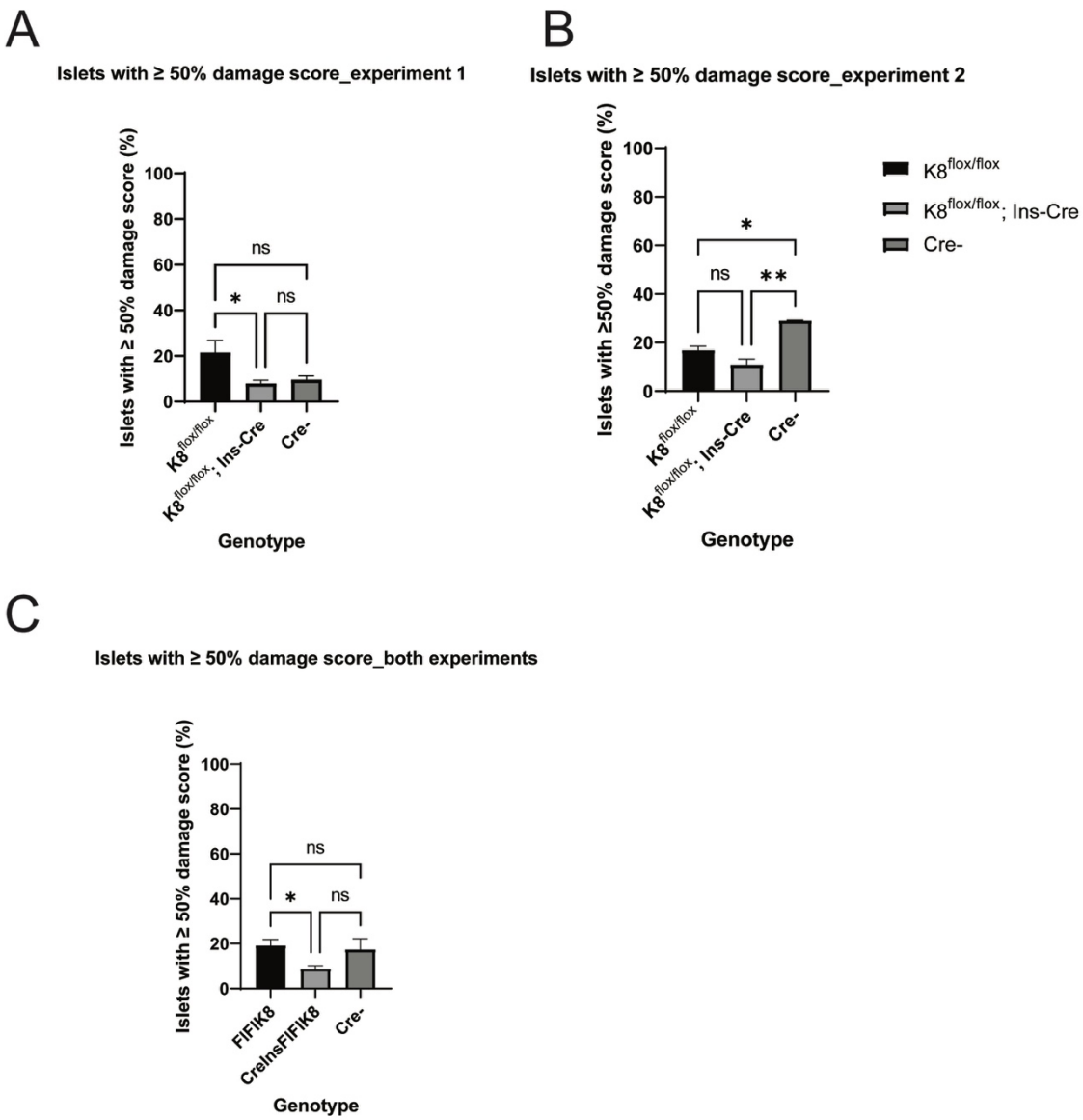

Figure 19: Highly damaged islets are common in mice which express keratin 8 in β-cells than in conditional knockout mice**.** For the clarification of the islet damage score, islets with more than 50% damage (damage scores 3 and 4) were taken into consideration and further analyzed. There is more damage observed in K8 positive control compared to the conditional knockout and another control regarding the experiment 1 (A). The experiment 2 (B) shows more damage and diabetes susceptibility of Cre^- control mice than for control $K8^{flox/flox}$ mice. The summary of the experiment is shown on the right graph and it is pointing out that the conditional knockout mice are more resistant to streptozotocin exposure and diabetes than keratin-expressing mice. p-values (*<0.05, **<0.01)

For a better understanding of the islet damage score and to analyse levels of islet damage, frequency distribution graphs were made (Figures 20 and 21). The graphs related to frequency distribution explain what is the most common damage score and how can these results be further used to analyze the role of keratins. A graph representing frequency distribution with islets from experiment 1 (Figure 21) shows that most of the examined islets have up to 10% of damage. The trend for the islets follows in the next way: there is a lower percentage of islets with no damage at all, while the distribution of islets with

higher damage score decreases. In terms of damage score distribution between the mice, the islets belonging to $K8^{flox/flox}$; Ins-Cre mice are assigned with scores 0 and 1, for score 2 (up to 30% damage), there is a drop in distribution regarding $K8^{flox/flox}$; Ins-Cre mice. $K8^{flox/flox}$ mice have a bigger distribution of islets with higher damage score: islets with scores 2, 3, and 4, or islets with up to 30% and more than 50% are more frequent in $K8^{flox/flox}$ mice. For the islets from Cre^- mice it can be said that there is a high distribution for scores 1 and 2, while for the score 4 Cre^- mice have a slightly higher distribution compared to $K8^{flox/flox}$ mice. When it comes to the data related to experiment 2 (Figure 21), there is a streaking similarity in the distribution of islets with damage scores 0 and 1 for $K8^{flox/flox}$; Ins-Cre mice. A similar distribution can be seen for islets belonging to mice from $K8^{flox/flox}$ and Cre^- mice regarding score 1. Higher damage score is more common for Cre^- mice, where the frequency distribution graph shows the evidently higher distribution for Cre^- mice compared to the islets from other mice ($K8^{flox/flox}$ and $K8^{flox/flox}$; Ins-Cre).

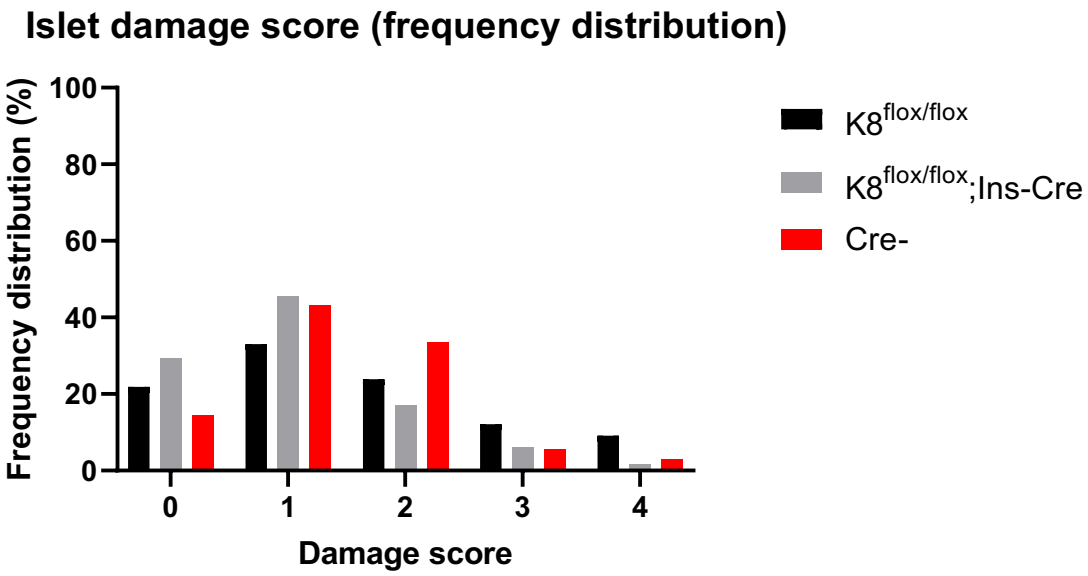

Figure 20: Frequency distribution for the islets of mice from experiment 1 shows a distribution pattern for all genotypes: the highest distribution for all islets is for damage score 1, and starts to decrease accordingly to the increase of a damage score value. The pace of change is different for $K8^{flox/flox}$ mice comparing to Cre^-: there is a slower decline of distribution for every damage score than in Cre^- mice.

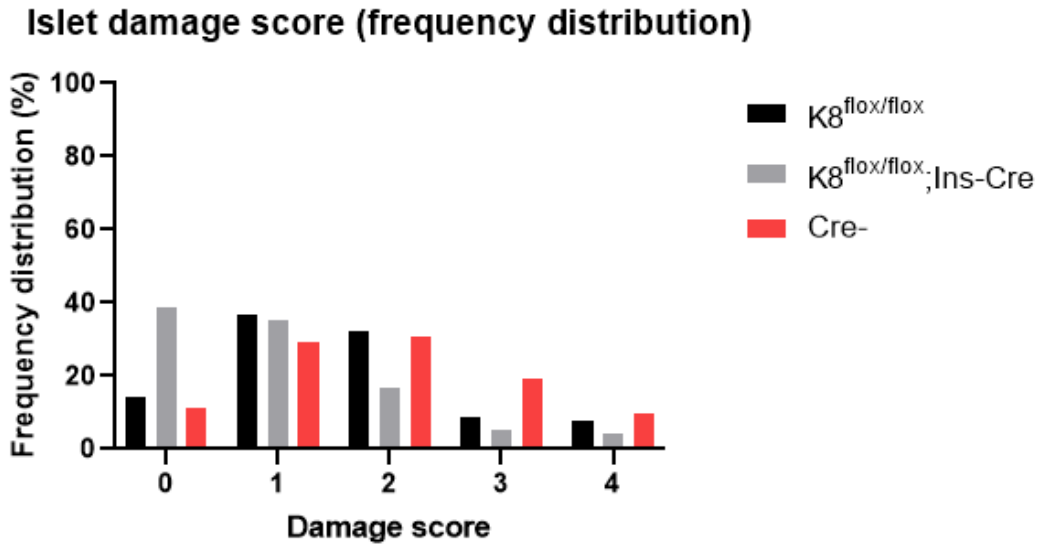

Figure 21: Frequency distribution for the islets of mice from experiment 2 shows a distribution pattern similar to the one from experiment 1. However, the distribution of islets from mice $K8^{flox/flox}$ and Cre^{-} is more or less equivalent for damage scores 1 and 2. There is a sharper decline in the distribution of islets with higher damage scores for $K8^{flox/flox}$ mice.

4.3.2. Streptozotocin treatment in $K8^{flox/flox}$; Ins-Cre mice does not lead to major changes in islet size

Islet size was also calculated and a possible change after diabetic stress was investigated. The graphs for experiment 1, experiment 2, and both experiments are shown below (Figures 22A, 22B, and 23). Islets analyzed in experiment 1 show no significant difference between genotypes (Figure 22A). For islets obtained from mice in experiment 2, it can be observed that the islet size in $K8^{flox/flox}$ is bigger compared with other genotypes (Figure 22B). The islet size in $K8^{flox/flox}$ mice can be explained by the presence of several islets that were extremely bigger than other observed ones. These islets were also characterized by a big degree of hemorrhage and damaged area with more than 50%. When running a comparison between conditional knockout and Cre^{-} mice, no significant difference is observed (Figure 22B). Both $K8^{flox/flox}$; Ins-Cre and Cre^{-} mice show significantly lower values than islets from mice in experiment 1. After compiling the data of two experiments into a single graph. However, a significant difference is seen between $K8^{flox/flox}$ and Cre^{-} mice (Figure 23).

In order to understand what size is the most common for the examined and analyzed islets, frequency distribution was run and related graphs were made (Figures 22A-23, right). The islets from mice in experiment 1 are characterized by a size in the range between 0 and 10000 μm^2 (Figure 23A, right), and as the area increases, the distribution of examined islets decreases. It can be also pointed out that the biggest islets can be found with values

of approximately 60000 μm^2, and they belong to K8$^{flox/flox}$; Ins-Cre and Cre$^-$, which can be seen on a frequency distribution graph. For experiment 2 (Figure 22B), right most of the islets have a smaller area on the graph, and this trend is emphasized for islets belonging to Cre$^-$ mice. It can be also observed that K8$^{flox/flox}$ mice have significantly bigger islets compared to other genotypes, which has been addressed previously. The reason for an extreme abundance of smaller islets for Cre$^-$ mice can be explained by small number of analyzed islets compared with the islets from other mice.

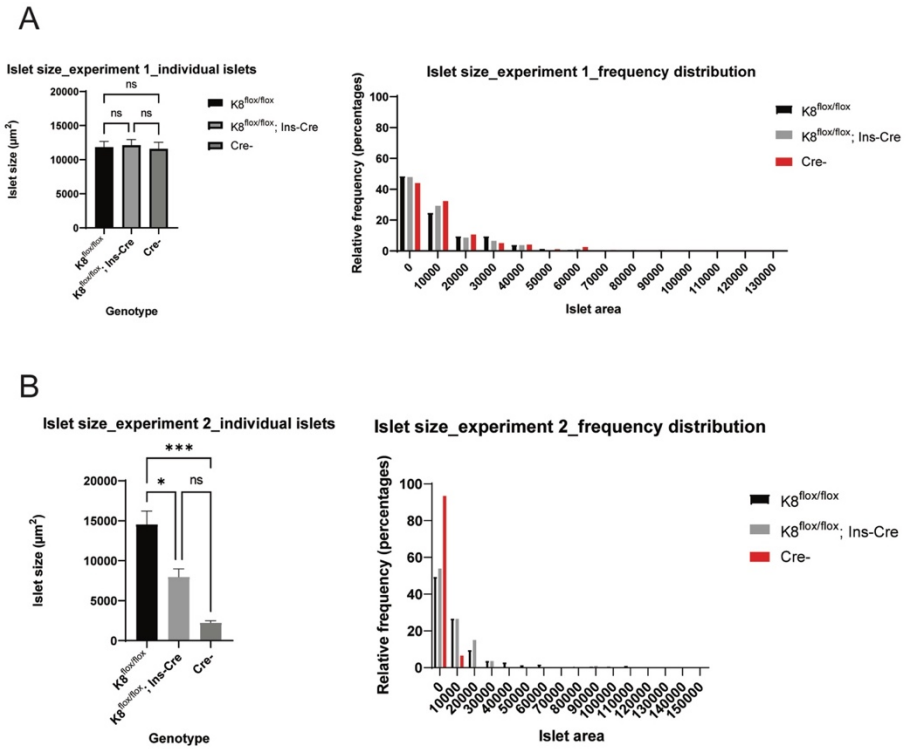

Figure 22: Islet size from the experiment 1 and the frequency distribution show that no significant (ns) difference occurs between the conditional knockout and controls (A). The results from experiment 2 show that the size of the islet decreases when mice are exposed to STZ and when K8 is knocked out (B). This result can raise different questions if the mice became diabetic or if there's anomaly in Cre$^-$ control. p-value (*<0.05 and ***<0.001).

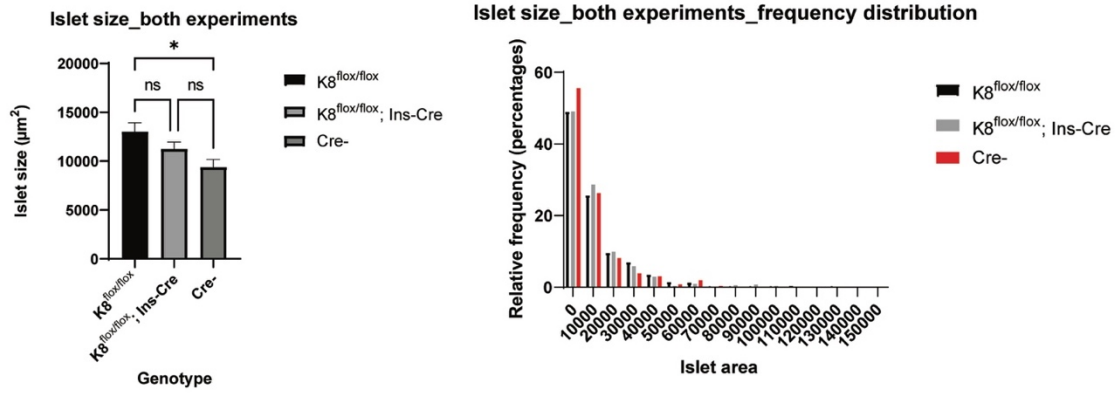

Figure 23: STZ-induced stress does not lead to a change in islet size between beta cell-specific K8 knockout and the controls. The final result shows that no significant difference in size is seen between the conditional knockout knockout (K8$^{flox/flox}$; Ins-Cre) and the controls (K8$^{flox/flox}$ and Cre$^-$). However, controls differ from each other. Most of the islets are characterized by an area in the range between 0 and 10000 μm^2 according to the frequency distribution graph shown on the right side of the figure. p-value (*<0.05).

4.3.3. $K8^{flox/flox}$ and $K8^{flox/flox}$; Ins-Cre mice show no difference in the islet mass and number upon STZ-induced stress

Islet mass (mass/section ratio) was also calculated for islets from mice in experiment 1 and experiment 2 as well as for the islets from both experiments combined. After compiling all data from experiment 1 (Figure 24A), the final result shows that the islet mass is not altered after STZ treatment. In other words, the high-dose STZ treatment did not lead to a more significant change/decrease of the islet mass. When it comes to frequency distribution, islets are characterized by lower islet mass values. However, there were bigger variations in islet mass between the groups. The values can be explained by the number of islets detected and analyzed and also the choice of sections with the most islets. It should be also emphasized that smaller islets were observed within the section (Figure 24B). The final result regarding the islet mass confirms that no significant difference is seen between the groups (Figure 25). Along with the analysis of islet mass, evaluation and the assessment of the islet number were done to observe if STZ-induced stress causes the decrease of the islet number. However, the statistical analysis of all the islets from experiment 1 (Figure 26A), experiment 2 (Figure 26B), and both experiments combined (Figure 26C) showed no significant difference in the islet number.

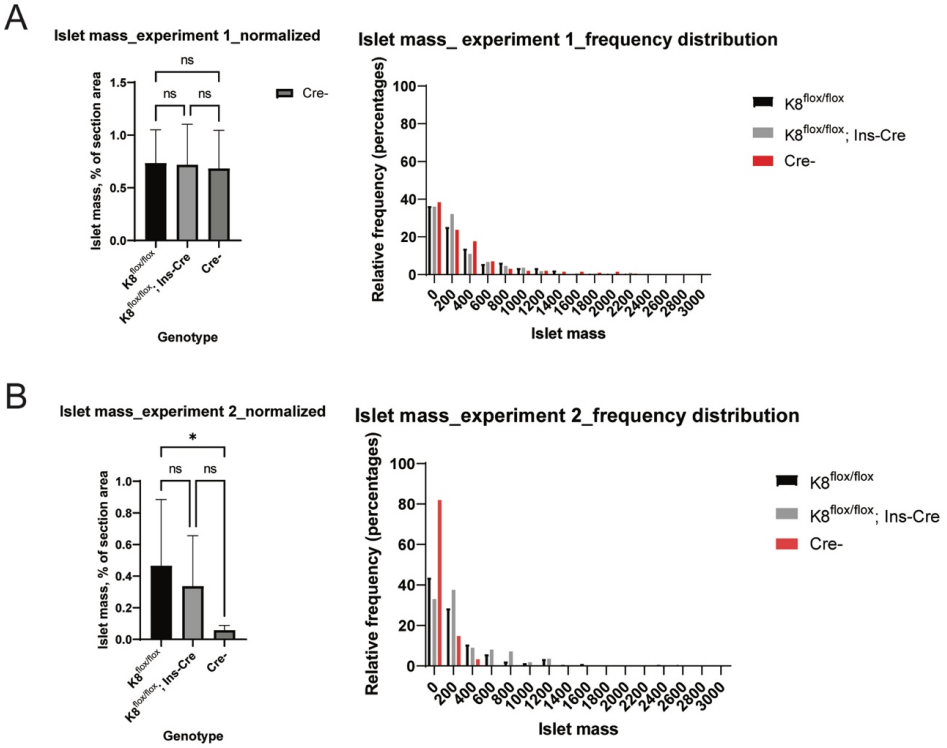

Figure 24: The final result of both experiments shows that no significant difference in islet mass is seen between the knockout ($K8^{flox/flox}$; Ins-Cre) and the controls. In experiment 1, islets do not differ between each other in the islet mass and most of them are characterized by lower mass according to the frequency distribution graph (A). In experiment 2, islets do not differ in mass when discussing or comparing the conditional knockout group and the controls. However, controls show significant difference between each other shown by the p-value. Also, most of the islets are characterized by lower islets mass seen in the frequency distribution graph (B). p-value (*<.0.05)

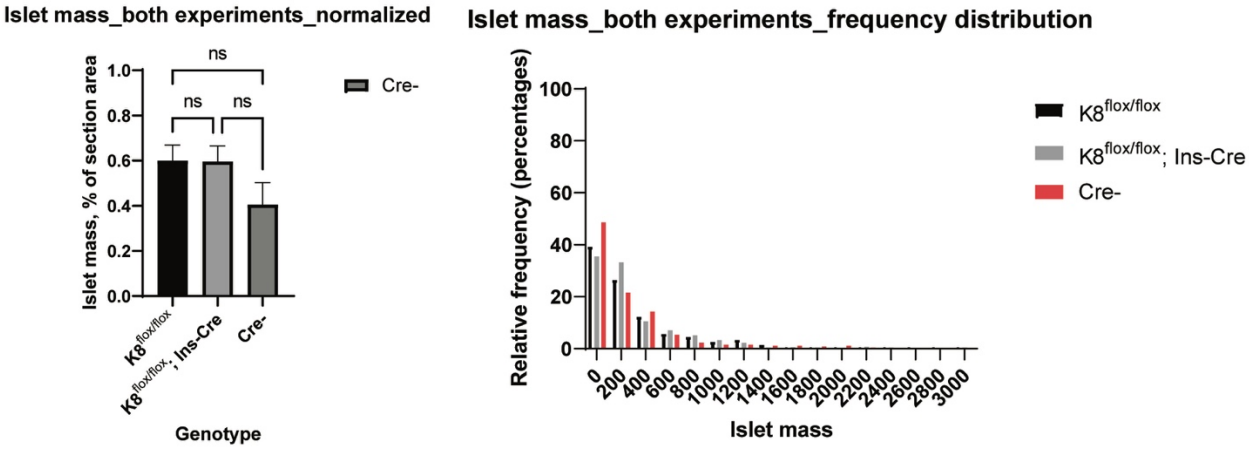

Figure 25: The final result of both experiments shows that no significant difference in islet mass is seen between the knockout ($K8^{flox/flox}$; Ins-Cre) and the controls. Due to the selection of pancreatic sections and availability of the islets, Cre^{-} shows lower but no significantly different islet mass.

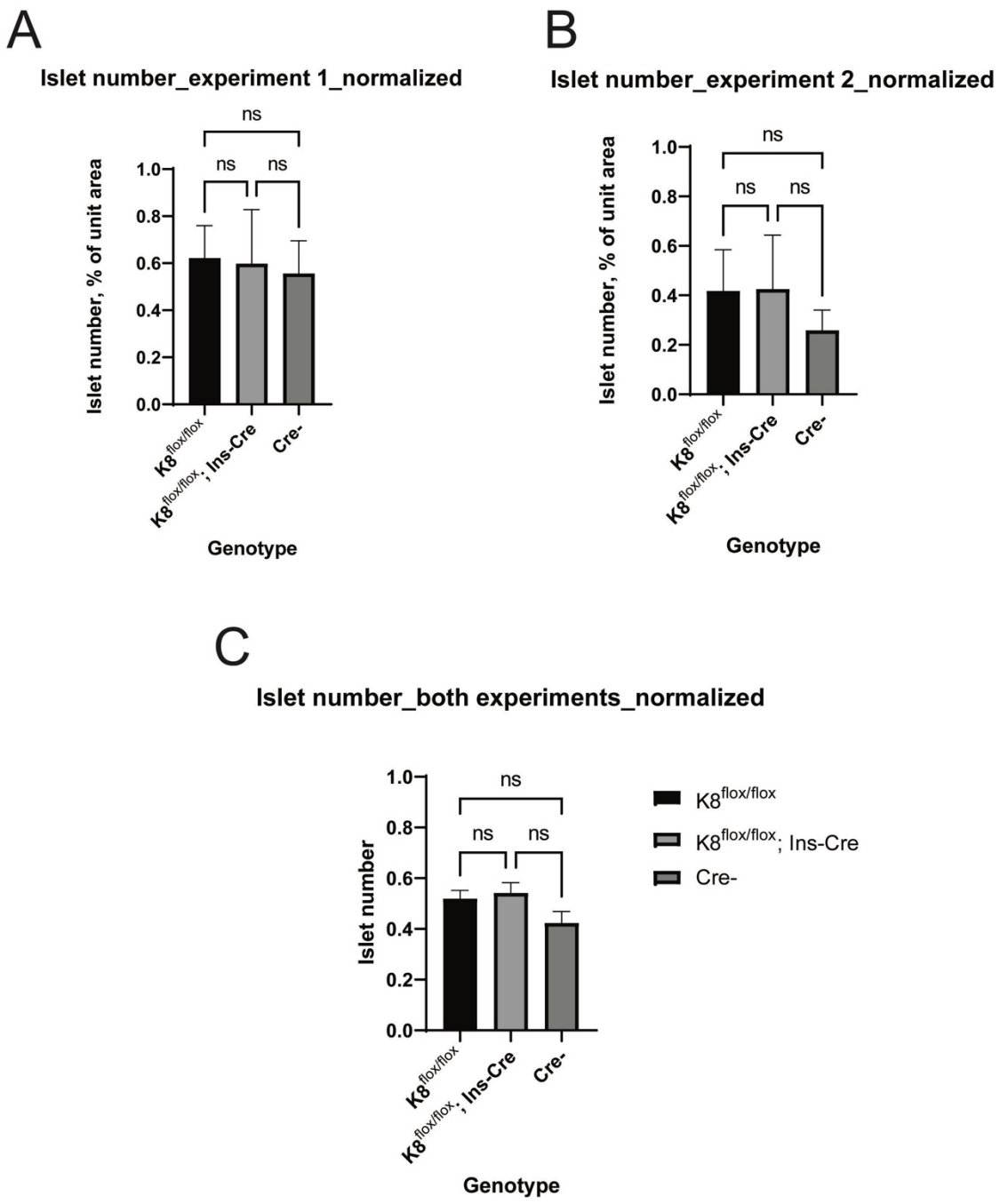

Figure 26: The final result of both experiments shows that no significant difference in islet number is seen between the knockout ($K8^{flox/flox}$; Ins-Cre) and the controls. No significant difference is seen in experiment 1 (A), experiment 2 (B), and after compiling the data from both experiments together (C).

4.4. GLUT2 is mistargeted from the membrane to the cytoplasm when K8 is absent in β-cells

The cellular GLUT2 localization in β-cell of the islets (Figure 27A) and the quantification thereof are shown in the figures below (Figure 27B). The graph shows the distribution of GLUT2 in β-cell for both $K8^{flox/flox}$ and $K8^{flox/flox}$; Ins-Cre (Figure 27B). The peak of the GLUT2 signal is located in the middle between the two nuclei which explains the

localization of GLUT2 on cell membranes of β-cells of $K8^{flox/flox}$ mice. For $K8^{flox/flox}$; Ins-Cre mice, the graph peaks are located towards the central parts of the cells, which shows that GLUT2 in conditional knockout mice has more cytosolic localization. The values of peak fluorescence intensities (Figure 28A) showed a significant difference (p=0.049) and confirmed the divergent distribution of GLUT2 in wild-type and conditional knockout mice. The content of GLUT2 in β-cells was calculated after measuring areas under curve (AUC) from Figure 27B and no significant difference between islets of $K8^{flox/flox}$ and $K8^{flox/flox}$; Ins-Cre mice was observed (Figure 28B). The graph presenting the area under the curve shows that the content of GLUT2 remains the same regardless of different distributions between $K8^{flox/flox}$ and $K8^{flox/flox}$; Ins-Cre mice. The principle of peak fluorescence intensity measurement is shown in Figure 27C.

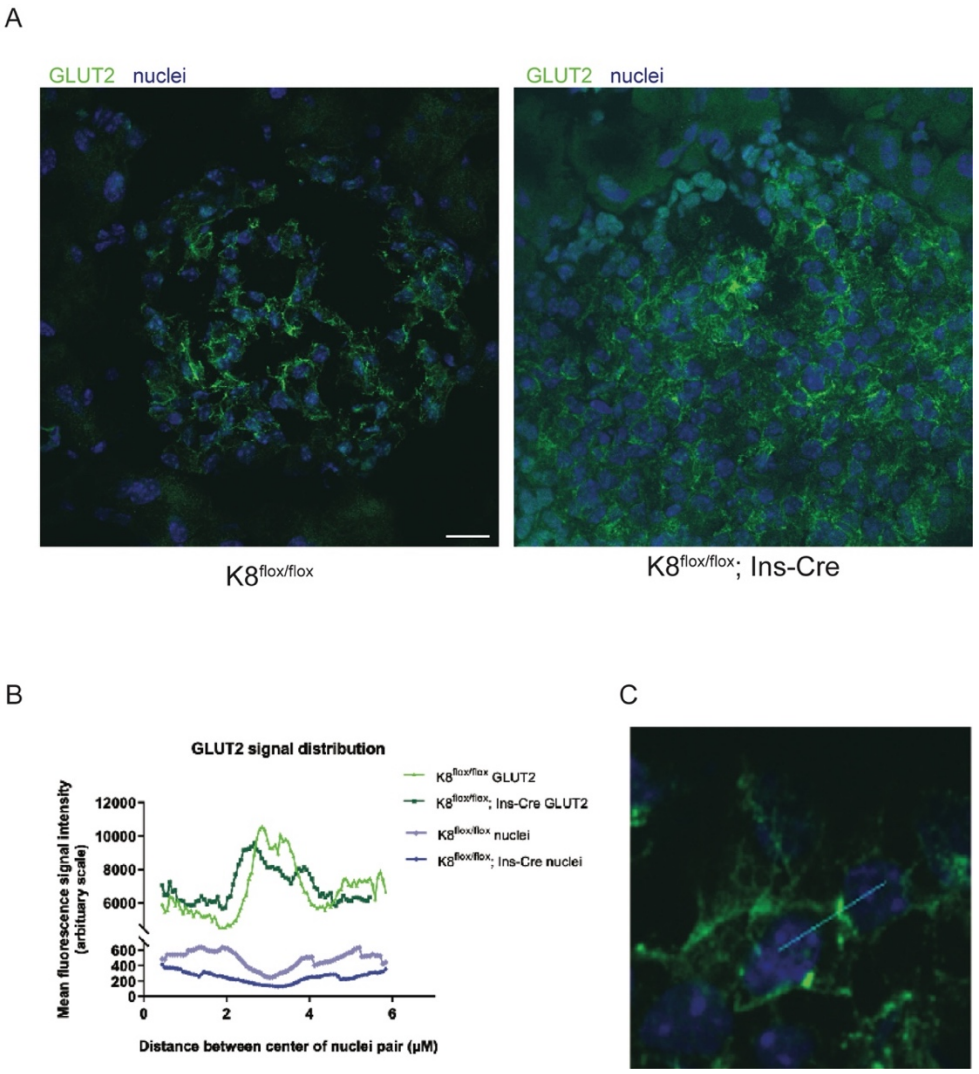

Figure 27: The knockout of keratin 8 in β-cells mistargets the GLUT2 in pancreatic islets. Images (A) show the localization of GLUT2 in control (left) and conditional knockout (right). It is seen that control or keratin-present β-cells GLUT2 is localized on the membrane, while the knockout of keratins leads to their translocation from membrane to the cytoplasm. This Is also confirmed by the graph for GLUT2 signal distribution (B); the blue graphs show signal distribution for the nuclei, while the green graphs correspond to GLUT2. The peak of the pale green ($K8^{flox/flox}$) graph is located exactly in the middle part, which corresponds to the membrane, while the peak of the dark green ($K8^{flox/flox}$; Ins-Cre) graph Is shifted toeards the peak of the blue nuclei which resemble the centres of the nuclei. The peak fluorescence intensity measurement was achieved by measuring the intensity for both GLUT2 and nuclei along the line that was drawn between neighboring nuclei (C).

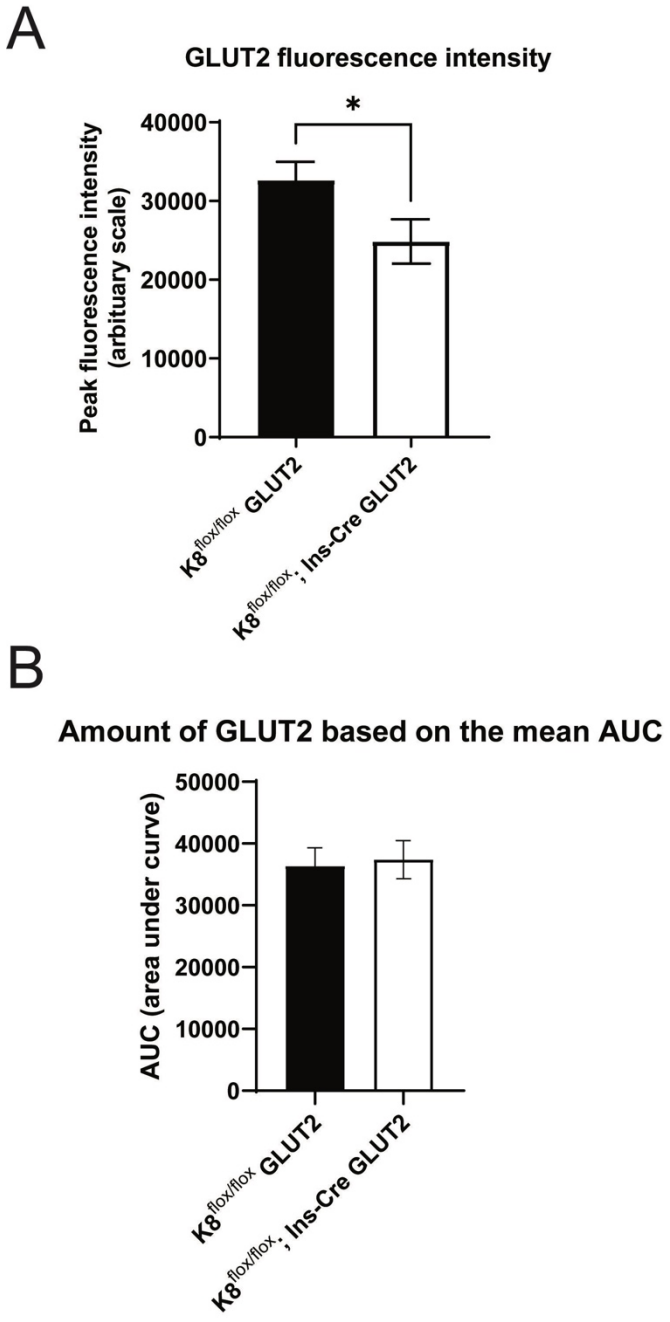

Figure 28: The mislocalization of GLUT2 is dependent on keratin content, not on GLUT2 itself. GLUT2 fluorescence intensity graph shows that GLUT2 is mistargeted from the membrane to the cytoplasm after eliminating keratin 8 from β-cells. (A). After running t-test, a statistical difference was observed (p=0.049) and indicates the mislocalization of GLUT2. To confirm that this is not dependent on content of GLUT2, area under curve (AUC) was calculated for both $K8^{flox/flox}$ and $K8^{flox/flox}$; Ins-Cre (B). After performing a statistical analysis, no significant difference was seen (p=0.2882), which indicates that the content of GLUT2 does not affect the mislocalization of GLUT2. P-value (*<0.05).

5. Discussion

5.1. Histological analysis of untreated mice

The endocrine pancreas counts up to 2% of the whole weight of the pancreas and most of the pancreatic weight accounts for the exocrine pancreas (up to 80%). Islets of Langerhans are usually in size between 50 and 500 μm and depending on the islets, up to 3000 cells can make a single islet (Alonso-Magdalena et al., 2019; Shi and Liu, 2014). A study with $K8^{flox/flox}$ and $K8^{flox/flox}$; Ins-Cre mice which was focused primarily on morphological properties of the islets (size, mass, and number), showed that the mice ($K8^{flox/flox}$; Ins-Cre) which lack K8 have bigger islets compared to the wild type ($K8^{flox/flox}$) (p-value 0.0055) (Baghestani and Haldin, unpublished). This finding was a main starting point to investigate if the proliferation occurs in the islets of Langerhans. To investigate the proliferation in β-cells, measurements related to cell and nucleus size first had to be done. Most of the islets analyzed were with a lower area and two separate measurements were done: for the islets with a size between 5000 and 14000 μm^2 and the islets with a size bigger than 14000 μm^2. The preliminary results showed that more large-sized islets (above 14000 μm^2) are more common in $K8^{flox/flox}$; Ins-Cre mice. For islets from the first category (islet area range between 5000 and 14000 μm^2), no difference was seen in cell size and nucleus size. After repeating the measurement and analysis for bigger islets, several points can be observed. The cell size is significantly bigger for the knockout mice than for the wild type. However, when it comes to the other parameters, no significant difference is seen between the mice. Regarding the nucleus size, if the individual values are compared with each other, then a trend in bigger nuclear size for $K8^{flox/flox}$ mice follows, as well as the probability for a bigger difference, due to the change in p-value. The result after analyzing individual nuclei was non-significant with the p-value being relatively close to 0.05 (0.0517). Another hypothesis for increased islet size would tell that the absence of keratins leads to an increase, but it can be due to the abundance of collagen in the extracellular matrix in the vicinity of the islets and within islets. Collagen is known for the interaction between islets and acinar cells. However, no difference could be observed. The phenomenon of bigger islets opens further questions and more research is expected to be done.

It should be kept in mind that the values of cell size and nucleus size were obtained using a cell detection tool from QuPath (Bankhead et al., 2017). Cell detection tool allows manual adjustments of nuclear and cellular parameters, however, after setting the adjustments, the outcome can be far from the ideal or real: for instance, some of the islet

cells can extrude into the exocrine pancreas and some of the nuclei are not counted or several nuclei are counted as a single one. Future work would consider coding in the Stardust script (Bankhead et al., 2017) which counts both the cell and nuclei accurately, but it requires time, experience, and patience.

5.2. Proliferation in β-cells

Proliferation in β-cells is characterized by a lower rate compared to the cells which are characterized by common stress exposure and metabolic demand, such as epithelial cells in the colon. β-cells are generally multiplied and formed during embryogenesis and their number remains the same after infancy (Shcheglova et al., 2022). To assess the proliferation rate in cells or tissues of interest, proliferation markers and components involved in proliferation signalling are used, and in this case, Ki67, YAP, and β-catenin were analyzed. The hypothesis stated that the islets that lack K8 in β-cells are bigger and this finding was based on preliminary results of basal/untreated histology samples (Baghestani and Haldin, unpublished). The first approach to evaluate the proliferation analysis was to observe if there was a difference in the number of positive Ki67 cells in pancreatic islets. The results showed no difference between $K8^{flox/flox}$ and $K8^{flox/flox}$; Ins-Cre mice and the only Ki67-positive cells were usually located peripherally or in several cells inside the islet. Embryological research has shown that the Wnt signaling pathway is one of the significant processes that contribute to the complete development of the endocrine pancreas (Murtaugh, 2008). Also, it has been shown that the overexpression of E-cadherin in pancreatic islets allows adhesion of ß-cells and prevents translocation of β-catenin, a Wnt signaling component, to the nucleus by tethering to a cellular membrane (Wakae-Takada et al., 2013). Imaging of β-catenin was done to see if β-catenin is more distributed within the nucleus in conditional knockout mice than in $K8^{flox/flox}$ mice. The result shows no significant difference in the membranous distribution of β-catenin in β-cells of both genotypes and no difference or no bigger nuclear distribution is seen. YAP, a component of the Hippo signaling pathway, is known as a transcription factor, whose activation causes phosphorylation and further expression of genes responsible for cell proliferation (Uttagomol et al., 2019). Preliminary imaging results showed that YAP is more expressed in nuclei of ß-cells of $K8^{flox/flox}$; Ins-Cre than in $K8^{flox/flox}$ mice. It can be speculated that the tissue disorganization might contribute to the islet size, which was shown after analyzing the organization and distribution of E-cadherin in pancreatic islets. A second reason for the result is that the cell volume has not been considered for the Analysis of islet-related parameters, which considered only two-dimensional sections.

The next step would be to implement a script for 3D reconstruction of the tissue and include cell volume in the analysis.

5.3. High-dose streptozotocin exposure and its effect on islet features

Streptozotocin is an antibiotic that is known for its toxic effects on β-cells and is therefore used in diabetes research as a mouse model for T1D. β-cells that lack keratins are shown to be more resistant to streptozotocin-induced injury and delayed hyperglycemia after exposure to the same agent (Alam et al., 2013). It has been shown that global knockout of keratin 8 and simultaneous exposure to streptozotocin affect the physiology of organs involved in the glucose regulation (Ku et al., 2010). To validate the statement from Ku's study, the islet damage score was assessed and islet size, islet mass, and islet number were calculated and analyzed. In this thesis, the Cre-loxP model was used which should be able to answer the role of β-cell K8, since K8 is normally expressed in all other simple epithelial cells. The results confirmed the finding that the knockout mice ($K8^{flox/flox}$; Ins-Cre) are less susceptible to the damage caused by streptozotocin when compared with two control groups ($K8^{flox/flox}$ and Cre^-). Two datasets were analyzed in these experiments. Islets belonging to the first experiment show the pattern where conditional knockout mice have islets that are resistant and less susceptible to diabetes and streptozotocin-induced damage. Controls ($K8^{flox/flox}$ and Cre^-) have similar damage scores each other, which explains keratins and their effect on the damage score. However, islets of mice from experiment 2, show a similar pattern as well, but with a higher damage score for Cre^- mice compared to the ones from experiment 1. The result regarding experiment 2 can be explained by the number of analyzed islets which was small compared to experiment 1 (62 versus 194) and that Cre^- mice can exhibit anomalies in their phenotype after the generation using the Cre-loxP approach. The reason for this kind of result is not yet clarified, but it is assumed that the mice with Cre^- genotype show anomalous characteristics in terms of phenotype and physiology.

Another analysis was run which was needed to explain the correlation between higher damage scores (3 and 4, ≥50% damage) and the genotype of mice. Regarding experiment 1, no difference in higher damage score is seen between Cre^- and $K8^{flox/flox}$; Ins-Cre mice, but more damaged islets are present in $K8^{flox/flox}$ mice compared to the conditional knockout. When discussing data from experiment 2, Cre^- mice show more islet damage when compared with $K8^{flox/flox}$ and $K8^{flox/flox}$; Ins-Cre mice. Again, this result can be explained by a smaller number of available islets and the anomalies present in Cre^- mice.

An important consideration of the damage score assessment is that this approach is subjective and relies on the examiner's evaluation, experience, and intuition. A previous attempt to assess the islet damage score (Figure 29) was done for experiment 1 and it shows that a different examiner estimated that islets in the same set of samples (experiment 1) from $K8^{flox/flox}$ mice are damaged up to 30% (with the damage score 2) and these are more common than the other ones. Also, it is seen that Cre^{-} mice have the most islets with more than 50% damage (damage score 4) than the other ones. On the other hand, the results of the thesis show the lower distribution of these islets in this category, with $K8^{flox/flox}$ accounting for most of these islets. As it was mentioned, this approach is subjective, because examiners have different approaches. For example, the ratio of estimated void/damaged area and islet area may contribute to the outcome, along with the presence of erythrocytes (Figure 30).

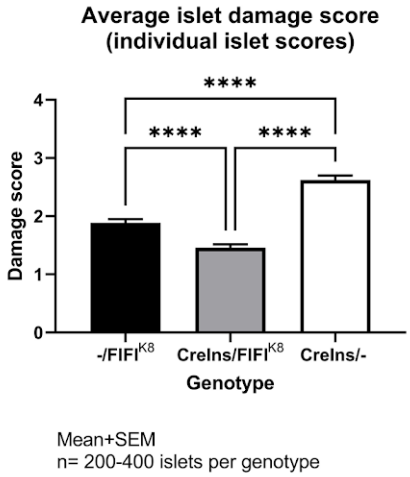

Figure 29: Previous attempt to assess the islet damage score after STZ treatment: the islets of conditional knockout ($K8^{flox/flox}$; Ins-Cre) mice are characterized by lower diabetes susceptibility. A previous assessment of the damage score for the islets analyzed in experiment 1. It can be seen that the difference in the damage score is significantly different between the genotypes and the lowest value can be found for the β-cell-specific conditional knockout. p-value (****<0.0001).

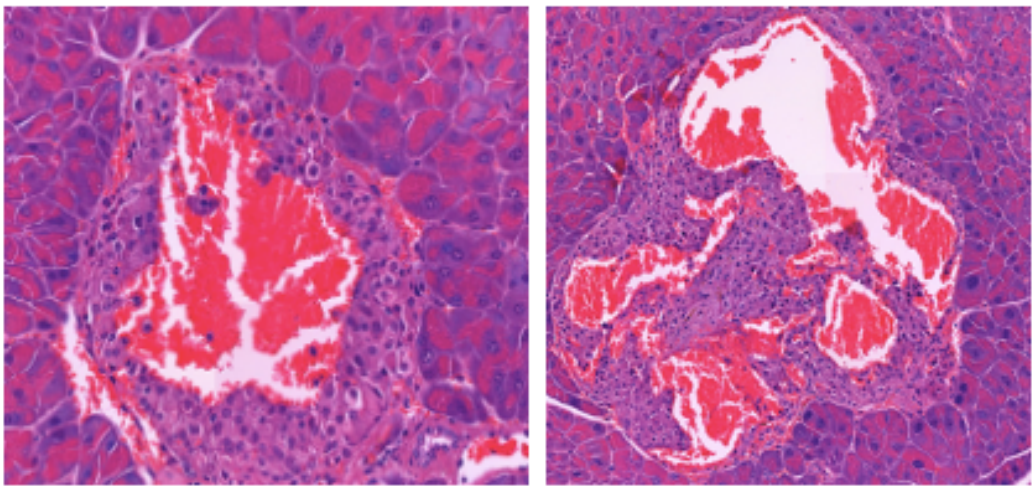

Figure 30: Islets with the abundant presence of erythovytes after STZ exposure**.** Several islets were found with a high degree of hemorrhage which explains diabetes susceptibility and higher damage score. Two islets with extreme damage are shown here. These islets can be an example for damage score 4 (more than 50% damage), where most of the area is filled with erythrocytes, and ruptured space can also be seen.

5.4. GLUT2 localization

Glucose transporter 2 (GLUT2) is the main transporter in mice involved in glucose uptake which leads to glucose-stimulated insulin secretion (GSIS) but is also significant in human glucose uptake along with GLUT 1 and GLUT3 (Berger and Zdzieblo, 2020). Another observation related to GLUT2 is that this transporter allows streptozotocin to enter β-cells (Hosokawa et al., 2001). It was previously shown that the global K8 knockout mice have a resistance to streptozotocin, due to the translocation of GLUT2 from the membrane to the cytosol (Alam et al., 2013). The peak fluorescence intensity values for GLUT2 show that GLUT2 is characterized by membranous distribution in $K8^{flox/flox}$ mice, while the knockout mice ($K8^{flox/flox}$; Ins-Cre) have a more cytosolic distribution of GLUT2 than on membranes. The mean area under the curve (AUC) shows that there is no difference in the content of GLUT2 between the genotypes. This finding shows that keratins might have a role in membrane targeting of GLUT 2, as stated by Alam et al. (Alam et al., 2013).

5.5. Concluding remarks

The islets from β-cell-specific conditional knockout mice are bigger, but the main reason is not known yet. The assessment of proliferation parameters has shown that no significant proliferation occurs in β-cells. Also, collagen levels were significantly small and no evidence that collagen contributes to the islet size is shown. It is still considered to do more research and work with YAP and younger mice because the trend follows that YAP is more distributed in nuclei of β-cell-specific conditional knockouts than in the control group.

Work related to diabetes susceptibility to streptozotocin exposure shows that the absence/knockout of keratins leads to lower islet damage and lower diabetes susceptibility. In terms of other parameters, such as islet size, islet mass, and islet number, no significant observations are seen. Regarding experiment 2 it should be considered that the size of β-cell-specific conditional knockout islets decreases and is smaller than the control group, which raises questions in terms of the streptozotocin effect on the islet size. The assessment of the islet damage score is a subjective approach, due to the different considerations, experiences, and perceptions of examiners or evaluators, and this kind of assessment is expected to use or implement an AI-based approach for a more accurate evaluation.

GLUT2 localization analysis confirmed that the knockout of keratin 8, leads to the translocation of GLUT2 in β-cell from the membrane to the cytoplasm. It is also shown that GLUT2 mislocalization is not influenced by or related to the amount of GLUT2 because GLUT2 has almost equal amounts in both membrane and cytoplasm. Keratins, therefore, might have a role in the targeting of β-cell GLUT2. Overall, the role of keratins in the physiology of β-cells is investigated and it is on the way to showing its further impact on glucose uptake and islet integrity.

6. Acknowledgments

After concluding my chapter of master's degree studies in Biomedical Imaging at the University of Turku, I would like to thank Diana Toivola for accepting me as a member of the Epithelial Biology Laboratory and approving me to do both internship and thesis. I must express my biggest gratitude to my supervisor Sarah Baghestani, who supervised and taught me new and useful methods. I want to thank the members of the Epithelial Biology Laboratory for the time spent, the support given and the friendships made during my stay in the laboratory. I also want to thank Lauri Polari, Catharina Alam, and Caroline Haldin for their advice and tips regarding the work with QuPath and pancreatic sections. Apart from the laboratory, I want to thank the staff of Turku Bioscience for training me on a 3i spinning disk confocal microscope and Pannoramic P1000 slide scanner and allowing me to do independent thesis work with these machines. I also want to thank professors, personnel, and classmates from my program and friends whom I met for making my stay in Turku unforgettable and valuable.

I want to thank my family, especially my stepdad, who was supportive and caring during my studies. I express gratitude to the people outside of Finland who sent messages of support which gave me confidence and made me determined to finish my master's degree. Finally, I want to dedicate this thesis to my mother, who unfortunately passed away in 2020 and would be happy and proud of the graduation.

7. References

Alam, C.M., S. Baghestani, A. Pajari, M.B. Omary, and D.M. Toivola. 2021. Keratin 7 Is a Constituent of the Keratin Network in Mouse Pancreatic Islets and Is Upregulated in Experimental Diabetes. *IJMS*. 22:7784. doi:10.3390/ijms22157784.

Alam, C.M., J.S.G. Silvander, E.N. Daniel, G.-Z. Tao, S.M. Kvarnström, P. Alam, M.B. Omary, A. Hänninen, and D.M. Toivola. 2013. Keratin 8 modulates β-cell stress responses and normoglycaemia. *Journal of Cell Science*. jcs.132795. doi:10.1242/jcs.132795.

Alam, C.M., J.S.G. Silvander, T.O. Helenius, and D.M. Toivola. 2018. Decreased levels of keratin 8 sensitize mice to streptozotocin-induced diabetes. *Acta Physiol*. 224:e13085. doi:10.1111/apha.13085.

Alonso-Magdalena, P., E. Tudurí, L. Marroquí, I. Quesada, R.M. Sargis, and A. Nadal. 2019. Toxic Effects of Common Environmental Pollutants in Pancreatic β-Cells and the Onset of Diabetes Mellitus. *In* Encyclopedia of Endocrine Diseases. Elsevier. 764–775.

Artner, I., B. Blanchi, J.C. Raum, M. Guo, T. Kaneko, S. Cordes, M. Sieweke, and R. Stein. 2007. MafB is required for islet β cell maturation. *Proc. Natl. Acad. Sci. U.S.A.* 104:3853–3858. doi:10.1073/pnas.0700013104.

Atkinson, M.A., M. Campbell-Thompson, I. Kusmartseva, and K.H. Kaestner. 2020. Organisation of the human pancreas in health and in diabetes. *Diabetologia*. 63:1966–1973. doi:10.1007/s00125-020-05203-7.

Bankhead, P., M.B. Loughrey, J.A. Fernández, Y. Dombrowski, D.G. McArt, P.D. Dunne, S. McQuaid, R.T. Gray, L.J. Murray, H.G. Coleman, J.A. James, M. Salto-Tellez, and P.W. Hamilton. 2017. QuPath: Open source software for digital pathology image analysis. *Sci Rep*. 7:16878. doi:10.1038/s41598-017-17204-5.

Baur, L.A., S.M. Twigg, and R.S. Magnusson eds. . 2012. A modern epidemic: expert perspectives on obesity and diabetes. Sydney University Press, Sydney. 432 pp.

Bell, G.I., S. Horita, and J.H. Karam. 1984. A Polymorphic Locus Near the Human Insulin Gene Is Associated with Insulin-dependent Diabetes Melliitus. *Diabetes*. 33:176–183. doi:10.2337/diab.33.2.176.

Berger, C., and D. Zdzieblo. 2020. Glucose transporters in pancreatic islets. *Pflugers Arch - Eur J Physiol*. 472:1249–1272. doi:10.1007/s00424-020-02383-4.

Block, J., V. Schroeder, P. Pawelzyk, N. Willenbacher, and S. Köster. 2015. Physical properties of cytoplasmic intermediate filaments. *Biochimica et Biophysica Acta (BBA) - Molecular Cell Research*. 1853:3053–3064. doi:10.1016/j.bbamcr.2015.05.009.

Chernyatina, A.A., D. Guzenko, and S.V. Strelkov. 2015. Intermediate filament structure: the bottom-up approach. *Current Opinion in Cell Biology*. 32:65–72. doi:10.1016/j.ceb.2014.12.007.

Dolenšek, J., M.S. Rupnik, and A. Stožer. 2015. Structural similarities and differences between the human and the mouse pancreas. *Islets*. 7:e1024405. doi:10.1080/19382014.2015.1024405.

Etienne-Manneville, S. 2018. Cytoplasmic Intermediate Filaments in Cell Biology. *Annu. Rev. Cell Dev. Biol.* 34:1–28. doi:10.1146/annurev-cellbio-100617-062534.

Ferrer, J., R. Gomis, J. Fernández Alvarez, R. Casamitjana, and E. Vilardell. 1993. Signals Derived From Glucose Metabolism Are Required for Glucose Regulation of Pancreatic Islet GLUT2 mRNA and Protein. *Diabetes*. 42:1273–1280. doi:10.2337/diab.42.9.1273.

Fiaschi-Taesch, N.M., F. Salim, J. Kleinberger, R. Troxell, I. Cozar-Castellano, K. Selk, E. Cherok, K.K. Takane, D.K. Scott, and A.F. Stewart. 2010. Induction of Human β-Cell Proliferation and Engraftment Using a Single G1/S Regulatory Molecule, cdk6. *Diabetes*. 59:1926–1936. doi:10.2337/db09-1776.

Georgia, S., and A. Bhushan. 2004. β cell replication is the primary mechanism for maintaining postnatal β cell mass. *J. Clin. Invest.* 114:963–968. doi:10.1172/JCI22098.

Gillespie, K.M. 2006. Type 1 diabetes: pathogenesis and prevention. *Canadian Medical Association Journal*. 175:165–170. doi:10.1503/cmaj.060244.

Gross, A., B. Zhou, L. Bewersdorf, N. Schwarz, G.M. Schacht, P. Boor, K. Hoeft, B. Hoffmann, E. Fuchs, R. Kramann, R. Merkel, R.E. Leube, and P. Strnad. 2022. Desmoplakin Maintains Transcellular Keratin Scaffolding and Protects From Intestinal Injury. *Cellular and Molecular Gastroenterology and Hepatology*. 13:1181–1200. doi:10.1016/j.jcmgh.2021.12.009.

Gunasekaran, U., C.W. Hudgens, B.T. Wright, M.F. Maulis, and M. Gannon. 2012. Differential regulation of embryonic and adult β cell replication. *Cell Cycle*. 11:2431–2442. doi:10.4161/cc.20545.

Herrera, P.L., V. Nepote, and A. Delacour. 2002. Pancreatic Cell Lineage Analyses in Mice. *ENDO*. 19:267–278. doi:10.1385/ENDO:19:3:267.

Herrmann, H., and U. Aebi. 2016. Intermediate Filaments: Structure and Assembly. *Cold Spring Harb Perspect Biol*. 8:a018242. doi:10.1101/cshperspect.a018242.

Herrmann, H., L. Kreplak, and U. Aebi. 2004. Isolation, Characterization, and In Vitro Assembly of Intermediate Filaments. *In* Methods in Cell Biology. Elsevier. 3–24.

Hohmann and Dehghani. 2019. The Cytoskeleton—A Complex Interacting Meshwork. *Cells*. 8:362. doi:10.3390/cells8040362.

Hol, E.M., and S. Etienne-Manneville. 2015. Editorial overview: Cell architecture: Intermediate filaments — from molecules to patients. *Current Opinion in Cell Biology*. 32:v–vi. doi:10.1016/j.ceb.2015.01.007.

Hosokawa, M., W. Dolci, and B. Thorens. 2001. Differential Sensitivity of GLUT1- and GLUT2-Expressing β Cells to Streptozotocin. *Biochemical and Biophysical Research Communications*. 289:1114–1117. doi:10.1006/bbrc.2001.6145.

Kim, H., M. Kim, S.-K. Im, and S. Fang. 2018. Mouse Cre-LoxP system: general principles to determine tissue-specific roles of target genes. *Lab Anim Res*. 34:147–159. doi:10.5625/lar.2018.34.4.147.

Ku, N.-O., D.M. Toivola, P. Strnad, and M.B. Omary. 2010. Cytoskeletal keratin glycosylation protects epithelial tissue from injury. *Nat Cell Biol*. 12:876–885. doi:10.1038/ncb2091.

Kulkarni, R.N. 2004. The islet β-cell. *The International Journal of Biochemistry & Cell Biology*. 36:365–371. doi:10.1016/j.biocel.2003.08.010.

Leung, P.S. 2010. Physiology of the Pancreas. *In* The Renin-Angiotensin System: Current Research Progress in The Pancreas. Springer Netherlands, Dordrecht. 13–27.

McLellan, M.A., N.A. Rosenthal, and A.R. Pinto. 2017. Cre- *lox* P-Mediated Recombination: General Principles and Experimental Considerations: Cre- *lox* P-Mediated Recombination. *Current Protocols in Mouse Biology*. 7:1–12. doi:10.1002/cpmo.22.

Moll, R., M. Divo, and L. Langbein. 2008. The human keratins: biology and pathology. *Histochem Cell Biol*. 129:705. doi:10.1007/s00418-008-0435-6.

Mueckler, M., and B. Thorens. 2013. The SLC2 (GLUT) family of membrane transporters. *Molecular Aspects of Medicine*. 34:121–138. doi:10.1016/j.mam.2012.07.001.

Murtaugh, L.C. 2008. The what, where, when and how of Wnt/β-catenin signaling in pancreas development. *Organogenesis*. 4:81–86. doi:10.4161/org.4.2.5853.

Nishimura, Y., K. Kasahara, and M. Inagaki. 2019. Intermediate filaments and IF-associated proteins: from cell architecture to cell proliferation. *Proc. Jpn. Acad., Ser. B*. 95:479–493. doi:10.2183/pjab.95.034.

Ohtsubo, K., M.Z. Chen, J.M. Olefsky, and J.D. Marth. 2011. Pathway to diabetes through attenuation of pancreatic beta cell glycosylation and glucose transport. *Nat Med*. 17:1067–1075. doi:10.1038/nm.2414.

Ohtsubo, K., S. Takamatsu, M.T. Minowa, A. Yoshida, M. Takeuchi, and J.D. Marth. 2005. Dietary and Genetic Control of Glucose Transporter 2 Glycosylation Promotes Insulin Secretion in Suppressing Diabetes. *Cell*. 123:1307–1321. doi:10.1016/j.cell.2005.09.041.

Omary, M.B., N.-O. Ku, P. Strnad, and S. Hanada. 2009. Toward unraveling the complexity of simple epithelial keratins in human disease. *J. Clin. Invest.* 119:1794–1805. doi:10.1172/JCI37762.

Pan, X., R.P. Hobbs, and P.A. Coulombe. 2013. The expanding significance of keratin intermediate filaments in normal and diseased epithelia. *Current Opinion in Cell Biology*. 25:47–56. doi:10.1016/j.ceb.2012.10.018.

Pekny, M., and E.B. Lane. 2007. Intermediate filaments and stress. *Experimental Cell Research*. 313:2244–2254. doi:10.1016/j.yexcr.2007.04.023.

Rachdaoui, N. 2020. Insulin: The Friend and the Foe in the Development of Type 2 Diabetes Mellitus. *IJMS*. 21:1770. doi:10.3390/ijms21051770.

Roep, B.O., S. Thomaidou, R. van Tienhoven, and A. Zaldumbide. 2021. Type 1 diabetes mellitus as a disease of the β-cell (do not blame the immune system?). *Nat Rev Endocrinol*. 17:150–161. doi:10.1038/s41574-020-00443-4.

Rorsman, P., and M. Braun. 2013. Regulation of Insulin Secretion in Human Pancreatic Islets. *Annu. Rev. Physiol.* 75:155–179. doi:10.1146/annurev-physiol-030212-183754.

Segerstolpe, Å., A. Palasantza, P. Eliasson, E.-M. Andersson, A.-C. Andréasson, X. Sun, S. Picelli, A. Sabirsh, M. Clausen, M.K. Bjursell, D.M. Smith, M. Kasper, C. Ämmälä, and R. Sandberg. 2016. Single-Cell Transcriptome Profiling of Human Pancreatic Islets in Health and Type 2 Diabetes. *Cell Metabolism*. 24:593–607. doi:10.1016/j.cmet.2016.08.020.

Shcheglova, E., K. Blaszczyk, and M. Borowiak. 2022. Mitogen Synergy: An Emerging Route to Boosting Human Beta Cell Proliferation. *Front. Cell Dev. Biol.* 9:734597. doi:10.3389/fcell.2021.734597.

Shi, C., and E. Liu. 2014. Anatomy, Histology, and Function of the Pancreas. *In* Pathobiology of Human Disease. Elsevier. 2229–2242.

Silvander, J.S.G., S.M. Kvarnström, A. Kumari-Ilieva, A. Shrestha, C.M. Alam, and D.M. Toivola. 2017. Keratins regulate β-cell mitochondrial morphology, motility, and homeostasis. *FASEB j.* 31:4578–4587. doi:10.1096/fj.201700095R.

Snider, N.T., and M.B. Omary. 2014. Post-translational modifications of intermediate filament proteins: mechanisms and functions. *Nat Rev Mol Cell Biol*. 15:163–177. doi:10.1038/nrm3753.

Stenvall, C.-G.A., J.H. Nyström, C. Butler-Hallissey, T. Jansson, T.R.H. Heikkilä, S.A. Adam, R. Foisner, R.D. Goldman, K.M. Ridge, and D.M. Toivola. 2022. Cytoplasmic keratins couple with and maintain nuclear envelope integrity in colonic epithelial cells. *MBoC*. 33:ar121. doi:10.1091/mbc.E20-06-0387.

Strnad, P., N. Guldiken, T.O. Helenius, J.O. Misiorek, J.H. Nyström, I.A.K. Lähdeniemi, J.S.G. Silvander, D. Kuscuoglu, and D.M. Toivola. 2016. Simple Epithelial Keratins. *In* Methods in Enzymology. Elsevier. 351–388.

Styers, M.L., A.P. Kowalczyk, and V. Faundez. 2005. Intermediate Filaments and Vesicular Membrane Traffic: The Odd Couple's First Dance?: Protein Targeting Regulation by Intermediate Filaments. *Traffic*. 6:359–365. doi:10.1111/j.1600-0854.2005.00286.x.

Thorens, B., D. Tarussio, M.A. Maestro, M. Rovira, E. Heikkilä, and J. Ferrer. 2015. Ins1 Cre knock-in mice for beta cell-specific gene recombination. *Diabetologia*. 58:558–565. doi:10.1007/s00125-014-3468-5.

Timofeev, V.I., R.N. Chuprov-Netochin, V.R. Samigina, V.V. Bezuglov, K.A. Miroshnikov, and I.P. Kuranova. 2010. X-ray investigation of gene-engineered human insulin crystallized from a solution containing polysialic acid. *Acta Crystallogr F Struct Biol Cryst Commun*. 66:259–263. doi:10.1107/S1744309110000461.

Toivola, D.M., P. Boor, C. Alam, and P. Strnad. 2015. Keratins in health and disease. *Current Opinion in Cell Biology*. 32:73–81. doi:10.1016/j.ceb.2014.12.008.

Toivola, D.M., P. Strnad, A. Habtezion, and M.B. Omary. 2010. Intermediate filaments take the heat as stress proteins. *Trends in Cell Biology*. 20:79–91. doi:10.1016/j.tcb.2009.11.004.

Toivola, D.M., G.-Z. Tao, A. Habtezion, J. Liao, and M.B. Omary. 2005. Cellular integrity plus: organelle-related and protein-targeting functions of intermediate filaments. *Trends in Cell Biology*. 15:608–617. doi:10.1016/j.tcb.2005.09.004.

Uttagomol, J., U.S. Ahmad, A. Rehman, Y. Huang, A.C. Laly, A. Kang, J. Soetaert, R. Chance, M.-T. Teh, J.T. Connelly, and H. Wan. 2019. Evidence for the Desmosomal Cadherin Desmoglein-3 in Regulating YAP and Phospho-YAP in Keratinocyte Responses to Mechanical Forces. *IJMS*. 20:6221. doi:10.3390/ijms20246221.

Wakae-Takada, N., S. Xuan, K. Watanabe, P. Meda, and R.L. Leibel. 2013. Molecular basis for the regulation of islet beta cell mass in mice: the role of E-cadherin. *Diabetologia*. 56:856–866. doi:10.1007/s00125-012-2824-6.

Westermark, P., E. Wilander, G.T. Westermark, and K.H. Johnson. 1987. Islet amyloid polypeptide-like immunoreactivity in the islet B cells of Type 2 (non-insulin-dependent) diabetic and non-diabetic individuals. *Diabetologia*. 30:887–892. doi:10.1007/BF00274799.

8. Supplementary material

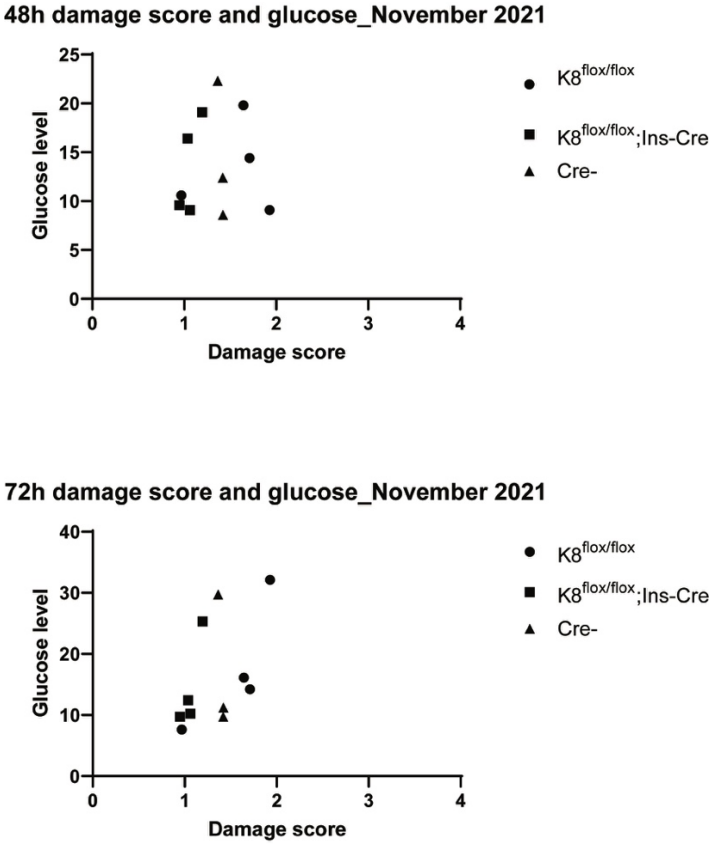

Supplementary figure 1: Blood glucose levels measured after 48 and 72 hours and the corresponding damage scores from mice in experiment 1 H). No correlation was observed between glucose levels and damage score.

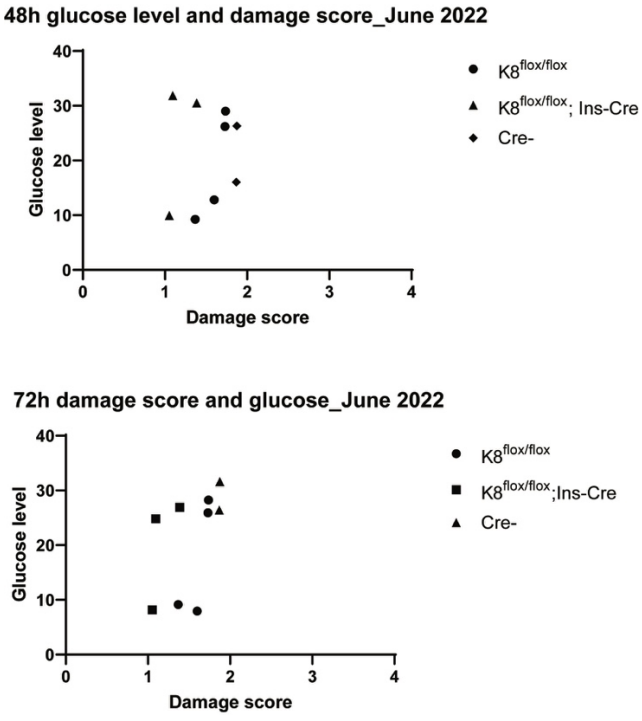

Supplementary figure 2: Glucose levels measured after 48 and 72 hours and the corresponding damage scores from mice in experiment 2. No correlation was observed between glucose levels and damage score.